

## Energy and angular distributions of autoionization electrons and channel interaction effects for the Sr $5pns$ $J=1$ autoionizing series

Yifu Zhu, Emily Y. Xu, and T. F. Gallagher

*Department of Physics, University of Virginia, Charlottesville, Virginia 22901*

(Received 23 April 1987)

A comprehensive experimental study of the energy and angular distributions of electrons ejected from the Sr  $5p_{3/2}ns_{1/2}$  and  $5p_{1/2}ns_{1/2}$   $J=1$  autoionizing states with  $n$  ranging from 10 to 20 has been performed using multistep laser excitation and time-of-flight electron spectroscopy. The branching ratios for autoionization to the available Sr<sup>+</sup> ion cores have been determined as well as the asymmetry parameter,  $\beta$ , of the electron angular distributions. Both the branching ratios and the  $\beta$  parameters are constant across isolated autoionizing states. However, measured  $\beta$  values and branching ratios change sharply across the line profiles of those  $5p_{3/2}ns_{1/2}$  states which have strong localized interactions with  $5p_{1/2}ns_{1/2}$  and  $5p_{1/2}nd_{3/2}$  states. A consistent six-channel quantum-defect-theory model has been developed which enables us to reproduce quite well the level positions, the total autoionization rates, the branching ratios to different Sr<sup>+</sup> ion states, and the angular distributions of the electrons ejected in the autoionization to the Sr<sup>+</sup>  $5s_{1/2}$  and  $5p_{1/2}$  ion states.

### I. INTRODUCTION

One of the most interesting aspects of the spectra of the alkaline-earth atoms arises from the fact that most of the doubly excited states are autoionizing states, which exhibit configuration interaction in two distinct ways. One is the interaction of discrete states with the continuum, and the other is the interaction of two or more autoionizing series with each other. Usually the excitation of an isolated autoionizing state leads to an asymmetric Beutler-Fano profile,<sup>1</sup> and the angular distribution of the ejected electrons changes dramatically across the line profile. Both are manifestations of the interference between the excitation to the continuum and bound parts of an autoionizing state.<sup>2,3</sup> If two or more autoionizing series interact with each other in the region of the excitation, the situation is even more complicated; consequently the quantitative analysis is difficult. To avoid these complexities, the experimental method of isolated core excitation (ICE) has been developed which results in relatively large cross sections for the excitation of a well-defined autoionizing state with negligible continuum excitation.<sup>4</sup> There are several advantages of this method. First, the excitation of an isolated autoionizing state leads to a simple Lorentzian profile, because there is virtually no continuum excitation. Second, the total angular momentum of the final autoionizing state can be monitored by the number of photons absorbed and the polarizations of the incident light. Third, all transitions driven are resonant single-electron-single-photon transitions, which are easily identified. Finally, the angular distribution of the ejected electrons does not vary across an isolated autoionizing state because there is no interference between bound and continuum excitations. For data analysis the theoretical methods of multichannel quantum-defect theory (MQDT) have been well

developed and successfully utilized to treat interacting Rydberg series and their corresponding continua.<sup>5-9</sup> This theory describes many atomic properties, including interseries interaction, in terms of a few relatively energy-independent parameters.

Extensive experimental studies of autoionizing Rydberg series of several alkaline-earth atoms have been reported.<sup>10-13</sup> Most of them have been focused on the level positions, the total autoionizing rates, and the manifestation of the interaction of the different autoionizing series in the excitation spectra. These experiments did not provide any information about the final states of the ion core or of the ejected electrons. To reach a detailed understanding of the dynamics of the autoionization, it is necessary to go beyond these measurements. Specifically, knowledge of the energy and angular distributions of the autoionizing electrons is required. The energy distribution of the ejected electrons is of course equivalent to the distribution of final ion states. In addition to the intrinsic interest, the branching ratios to excited ion states play a key role in, for example, dielectronic recombination in plasmas and short-wavelength laser development. Thus far, few experiments have been reported for the angular distributions and branching ratios of the electrons ejected from autoionizing states. In particular only the Ba  $6p_{3/2}ns_{1/2}$  and  $6p_{1/2}ns_{1/2}$   $J=1$  autoionizing states have been studied.<sup>14-16</sup>

Recently we reported the level positions and total autoionization rates of Sr  $5p_{3/2}ns_{1/2}$  and  $5p_{1/2}ns_{1/2}$   $J=1$  autoionizing states for  $n$  ranging from 10 to 20.<sup>17</sup> In this paper, we present results of extensive measurements of the angular distributions and branching ratios of the electrons ejected from these two autoionizing series. A novel aspect of these measurements is that for the Sr  $5p_{3/2}ns_{1/2}$  states, which overlap with some  $5p_{1/2}ns_{1/2}$  and  $5p_{1/2}nd_{3/2}$  states within the line profiles, the asym-

metry parameter  $\beta_{5s_{1/2}}$  for autoionization to the  $\text{Sr}^+5s_{1/2}$  ion state varies noticeably across the line profiles. The sharp dips of  $\beta_{5s_{1/2}}$  at the locations of the  $5p_{1/2}ns_{1/2}$  and  $5p_{1/2}nd_{3/2}$  states are clearly due to the discrete-discrete interactions of these autoionizing series. Analogous variations in the branching ratios to final  $\text{Sr}^+$  ion states are observed at the locations of the  $5p_{1/2}ns_{1/2}$  and  $5p_{1/2}nd_{3/2}$  states. For the first time, we present a unified six-channel MQDT analysis in terms of 14 energy-independent parameters: three eigenchannel quantum defects, five  $R$ -matrix elements, and six continuum transformation  $U$ -matrix elements. This approach enables us to reproduce quite well the level positions, the total autoionization rates, the branching ratios of different  $\text{Sr}^+$  states, and the angular distributions of the electrons ejected in the autoionization to the  $\text{Sr}^+5s_{1/2}$  and  $5p_{1/2}$  ion states.

In the following sections, we describe our experimental approach, the experimental results, the MQDT analysis, and the conclusions which may be drawn from this work.

## II. EXPERIMENTAL METHOD

The experiments were performed by exciting ground-state Sr atoms in a thermal beam with three pulsed tunable dye lasers to the autoionizing  $5pns$  states and observing the energy- and angle-resolved ejected electrons. As shown by Fig. 1, there are three possible electron energies for the autoionization of the  $5p_{3/2}19s_{1/2}$  state,

corresponding to autoionization to the  $5s_{1/2}$ ,  $4d_j$ , and  $5p_{1/2}$  states of  $\text{Sr}^+$ . Thus the electron-energy distribution gives the branching ratios to the available  $\text{Sr}^+$  final states, and the electron angular distribution, relative to the polarization of the exciting light, determines, to the extent possible, the partial waves of the departing electrons.

The experimental arrangement used for the measurements is shown in Fig. 2. An effusive Sr atomic beam produced by a resistively heated oven was collimated and passed between plates 2 and 3 which were separated by 1.0 cm. Its density at the interaction region between the plates 2 and 3 was estimated to be about  $10^8$  atoms/cm<sup>3</sup>. The three tunable laser pulses were produced by three dye lasers all pumped by the 355-nm third harmonic of a Quanta-Ray DCR-2 Nd:YAG laser, operating at 20 Hz (where YAG denotes yttrium aluminum garnet). The dye lasers had a pulse duration of about 5 ns, linewidth less than  $1\text{ cm}^{-1}$ , and energies of about  $100\ \mu\text{J}$  per pulse. The three almost collinear laser beams were linearly polarized and focused to a spot about 2 mm in diameter at the interaction region between plates 2 and 3, where they intercepted the Sr beam at a right angle, as shown by Fig. 2. Consider the excitation of the  $5p_{3/2}19s_{1/2}$  state, shown in Fig. 1. The first laser pumped the Sr  $5s^2\ ^1S_0$ - $5s5p\ ^1P_1$  transition at  $4609\ \text{\AA}$ , while the second dye laser pumped the Sr  $5s5p\ ^1P_1$ - $5s19s\ ^1S_0$  transition at  $4203\ \text{\AA}$ . A 10-ns delay in the second laser beam ensured that when it arrived at the interaction region the Sr  $5s5p\ ^1P_1$  state was already populated. The third dye laser, at wavelength  $4080\ \text{\AA}$ , excited the spherically symmetric Sr  $5s19s\ ^1S_0$  state to the autoionizing  $5p_{3/2}19s_{1/2}\ J=1$  state. If the third laser was tuned to  $4210\ \text{\AA}$  the  $5p_{1/2}19s_{1/2}$  state would be excited. A 50-ns delay between the first-laser and the third-laser pulses ensured that any coincidental two-photon ionization signal due to the first and third lasers

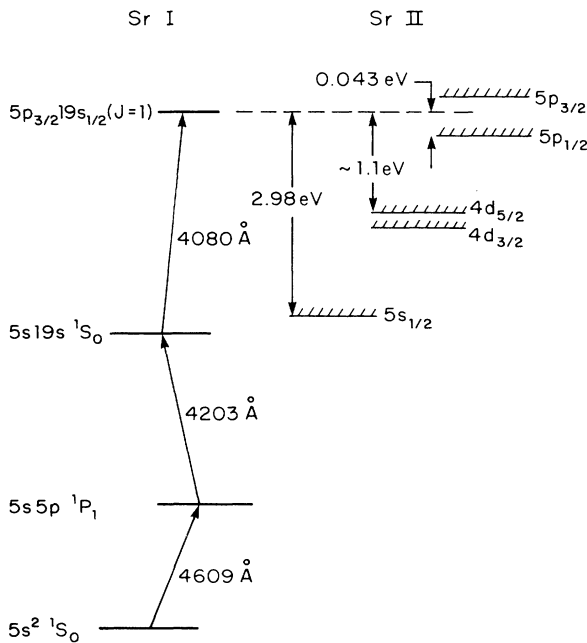


FIG. 1. Three-photon excitation scheme used to populate Sr  $5p_{3/2}ns_{1/2}$  or  $5p_{1/2}ns_{1/2}\ J=1$  autoionizing state. In the figure, the  $5p_{3/2}19s_{1/2}\ J=1$  state is populated, and the autoionization leads to  $\text{Sr}^+5p_{1/2}$ ,  $4d_j$ , and  $5s_{1/2}$  ion states. Correspondingly, different kinetic energies for the ejected electrons are also shown.

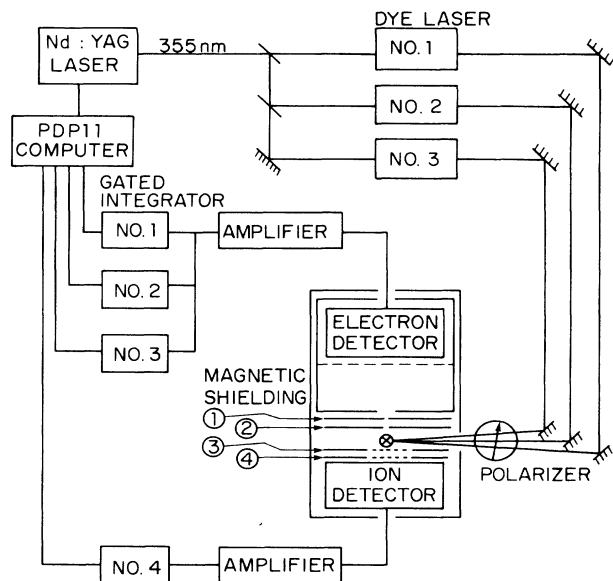


FIG. 2. Schematic of the experimental apparatus.

only could be completely suppressed. The ejected electrons were angle and energy resolved by a time-of-flight (TOF) spectrometer. The spectrometer consisted of a 25-cm-long Aerodag-coated aluminum drift tube mounted directly above the field-free interaction region and containing an electron detector which could be moved freely inside the drift tube to vary the effective drift length between 5 and 20 cm. The energy resolution,  $\Delta E$ , of the TOF spectrometer was  $\Delta E = 1.185E^{3/2}/L$ . Here  $L$  is the free drift length in cm and  $E$  is the electron kinetic energy in eV. Both the electron and ion detectors were dual microchannel plate detectors of the Comstock CP-602A type. The whole TOF spectrometer was enclosed by a  $\mu$ -metal magnetic shield to reduce the residual magnetic field to about 1 mG. The acceptance angle of the electron detector for electrons from the interaction region was defined by the diameter of the entrance aperture of the detector, 1.8 cm, and the free drift length  $L$ . With  $L = 18$  cm, the acceptance angle was  $6^\circ$ , and the maximum acceptance angle was  $20^\circ$ , corresponding to  $L = 5$  cm. The latter configuration was used to detect the low-energy electrons in the autoionization of Sr  $5p_{3/2}ns_{1/2}$  ( $n > 15$ ) states to the  $\text{Sr}^+ 5p_{1/2}$  ion core. In order to assure a field-free interaction region, plates labeled 1, 3, and 4 in Fig. 2 were directly grounded, and plate 2 was grounded through a 10-k $\Omega$  shunt resistor. The flight tube and the magnetic shielding were also grounded. 1  $\mu$ s after the laser pulses, long after all electrons had left the interaction region, a voltage pulse with peak value about 100 V was applied to plate 2, driving all  $\text{Sr}^+$  ions created into the ion detector, providing a convenient normalization for the differential electron signal. The outputs from the electron and ion detectors were amplified and recorded with Stanford Research Systems SR-250 gated integrators. One integrator was used to record the ion signal, and three others were used to record the three time resolved peaks of the electron signal, corresponding to the three possible electron energies. We show time resolved electron signals under several conditions in Fig. 3. After each shot of the laser the gated integrators were read by a PDP-11 computer. The signals were averaged by the computer over 1000 laser shots, and the data were stored in the computer for further analysis. As the TOF spectrometer was fixed in position, the angular distributions of the ejected electrons were obtained by rotating a double Fresnel rhomb half-wave retarder which changed the angle of the linear polarization of the incident third laser beam relative to the detection axis of the TOF spectrometer. The distribution was measured in a plane perpendicular to the direction of the propagation of the laser beams and containing the mutually perpendicular atomic beams and the detection axis.

All isolated  $5pns$  states exhibit the same angular distributions and branching ratios irrespective of where in the line profile they are excited. By "within the line profile" we mean over the energy range where the photoexcitation cross section is at least 20% of the peak value. Thus we have made the measurements reported here by exciting the center of the autoionizing state where the signal is the strongest. This is not the case for the

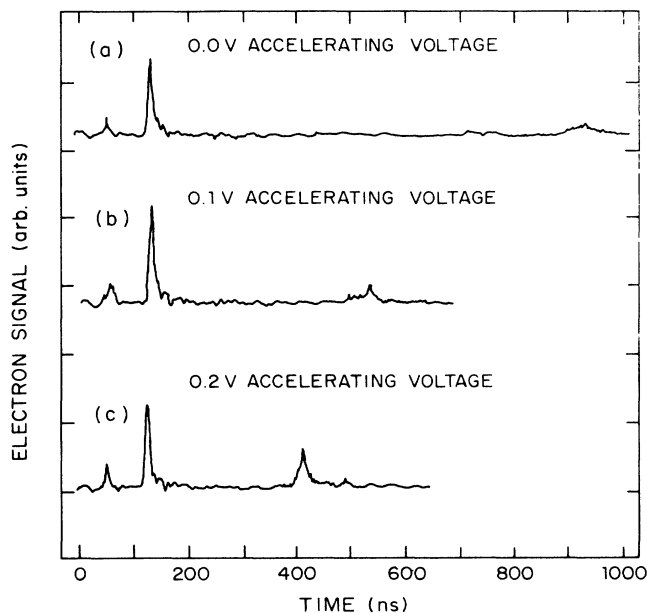


FIG. 3. Time-of-flight spectra of Sr  $5p_{3/2}20s_{1/2}$   $J=1$  autoionization electrons. The signals at 60, 120, and 920 ns correspond to autoionization to the  $\text{Sr}^+ 5s_{1/2}$ ,  $4d_j$ , and  $5p_{1/2}$  states. (a) No external accelerating field, (b)  $-0.1$  V accelerating voltage applied to grid plates 2 and 3, (c)  $-0.2$  V accelerating voltage applied to grid plates 2 and 3. The three peaks correspond to the decay into  $\text{Sr}^+ 5s_{1/2}$ ,  $4d$ , and  $5p_{1/2}$  continua, respectively.

$5p_{3/2}ns_{1/2}$  states which lie below the  $5p_{1/2}$  limit and exhibit strong interseries interactions with the degenerate  $5p_{1/2}ns_{1/2}$  and  $5p_{1/2}nd_{3/2}$  states. For these states, measurements were made across the entire line profile.

### III. EXPERIMENTAL OBSERVATIONS

Most of the data were taken in the manner used to obtain Fig. 3(a), with no accelerating voltages, so that the angular acceptance of the detector for 1.1- and 2.9-eV electrons is determined only by geometry and is the same for both cases. The variation of the electron signals at 60 and 120 ns with the angle  $\theta$  between the detection axis and the polarization direction of the third laser beam gives immediately the angular distributions of the 2.8- and 1-eV electrons, respectively. In Figs. 4 and 5 we show the angular distributions of the 2.8- and 1-eV electrons ejected from the autoionization of Sr  $5p_{1/2}14s_{1/2}$   $J=1$  state to the  $\text{Sr}^+ 5s_{1/2}$  and  $4d_j$  ion states. The dots represent the experimental data, the ratios of the electron signals to the ion signal, and the solid curves are the least squares fits to the expression

$$\frac{d\sigma}{d\Omega} = \frac{\sigma}{4\pi} [1 + \beta P_2(\cos\theta)]. \quad (1)$$

Here  $\beta$  is the asymmetry parameter,  $\sigma$  is the total cross section,  $P_2(\cos\theta)$  is the second-order Legendre polynomial, and  $\theta$  is the angle between the third laser po-

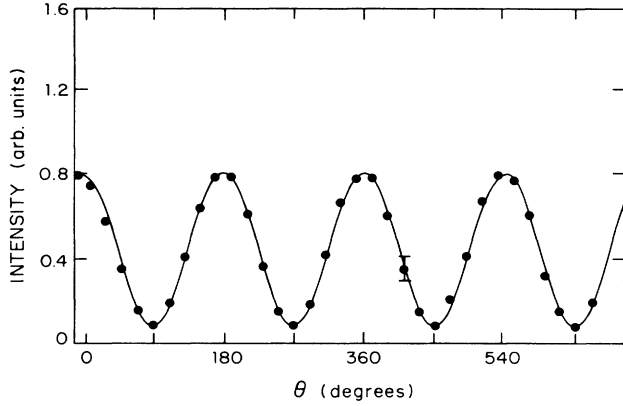


FIG. 4. Angular distribution of the 2.82-eV electrons ejected from the  $5p_{1/2}14s_{1/2}$  state to the  $\text{Sr}^+ 5s_{1/2}$  continuum, experimental data ( $\bullet$ ), least-squares fit to Eq. (1) (—).  $\theta$  is the angle between the detection axis and the linear polarization axis of the incident third laser beam.

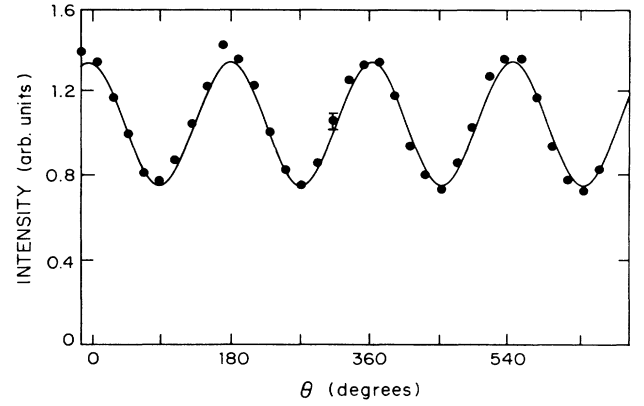


FIG. 5. Angular distribution of 1-eV electrons ejected from  $\text{Sr } 5p_{1/2}14s_{1/2} J=1$  state, autoionizing to the  $\text{Sr}^+ 4d$  ion states, experimental data ( $\bullet$ ), least-squares fit to Eq. (1) (—).  $\theta$  is as in Fig. 4.

larization and the momentum of the ejected electrons. It is consistent with Yang's theorem,<sup>18</sup> which implies that the electric dipole transition for the excitation to the autoionizing  $5p_{3/2}ns_{1/2}$  or  $5p_{1/2}ns_{1/2} J=1$  state starting from a spherically symmetric  $5sns \ ^1S_0$  Rydberg state leads only to Legendre polynomials of order 0 and 2 in the electron angular distribution.

Since no accelerating potential was applied and the electrons traveled along straight-line trajectories, the angular resolution and collection efficiencies are the same for the 1- and 2.8-eV electrons. This was checked by observing the intensity changes of the 1- and 2.8-eV electrons as functions of a small voltage applied between plates 2 and 3. The small stray field only affected electrons with kinetic energy of 50 meV or less appreciably. We may integrate the electron signals over the angle  $\theta$  to determine the relative probabilities of autoionization to the  $5s_{1/2}$  and  $4d_j$  ion cores. For states below the  $\text{Sr}^+ 5p_{1/2}$  limit these are the only available ion states,

and this is in fact the branching ratio.

For the  $5p_{3/2}ns_{1/2}$  states above the  $\text{Sr}^+ 5p_{1/2}$  limit the difficulties inherent in detecting the low-energy electrons produced in the autoionization to the  $\text{Sr}^+ 5p_{1/2}$  ion core require some additional effort to measure the branching ratios. We used two different techniques to measure the branching ratios. In the first we collected all the ions and the electrons corresponding to the  $5s_{1/2}$  and  $4d_j$  ion states at a free drift length  $L=18$  cm and  $\theta=0$ . These measurements, together with the known electron angular distributions, allowed us to calculate the ratio of the total electron signal for autoionization to the  $\text{Sr}^+ 5s_{1/2}$  and  $4d_j$  states to the total ion signal. We then reduced the free drift length to  $L=5$  cm, and applied a negative voltage to plate 3, to drive all low-energy electrons to the detector, and also detected the ions. At a voltage of about 2 V the collection efficiency for the electrons with a kinetic energy  $\leq 60$  meV was 100%. The effect of the small field produced,  $\sim 2$  V/cm, is negligible in the exci-

TABLE I. The asymmetry parameters  $\beta_{5s_{1/2}}, \beta_{4d_j}$  for  $\text{Sr } 5p_{1/2}ns_{1/2} J=1$  autoionizing states.

State	Experiment	Asymmetry parameters		Experiment
		$\beta_{5s_{1/2}}$	Theory	
$5p_{1/2}10s_{1/2}$	1.40(17)	0.80	0.60(22)	
$5p_{1/2}11s_{1/2}$	1.60(13)	1.70	0.40(14)	
$5p_{1/2}12s_{1/2}$	1.58(09)	1.27	0.40(13)	
$5p_{1/2}13s_{1/2}$	1.68(10)	1.80	0.68(17)	
$5p_{1/2}14s_{1/2}$	1.50(07)	1.10	0.42(12)	
$5p_{1/2}15s_{1/2}$	0.72(18)	1.60	0.36(14)	
$5p_{1/2}16s_{1/2}$	0.31(14)	1.00	0.30(13)	
$5p_{1/2}18s_{1/2}^a$	0.92(15)	1.50	0.42(16)	
$5p_{1/2}19s_{1/2}$	1.21(15)	1.70	0.48(13)	
$5p_{1/2}20s_{1/2}$	0.47(14)	1.20	0.37(13)	

<sup>a</sup>The  $5s17s \ ^1S_0$  state is degenerate with the  $5s17d \ ^1D_2$  state, and thus it is impossible to make unambiguous measurements for the  $5p_{1/2}17s_{1/2}$  state.

TABLE II. The branching ratios for Sr  $5p_{1/2}ns_{1/2}$   $J = 1$  autoionizing states.

State	Branching ratio to Sr <sup>+</sup> ion states (%)			
	$R_{5s_{1/2}}$		$R_{4d_j}$	
	Experiment	Theory	Experiment	Theory
$5p_{1/2}10s_{1/2}$	25(9)	16.5	75(9)	83.5
$5p_{1/2}11s_{1/2}$	18(4)	34.0	82(4)	66.0
$5p_{1/2}12s_{1/2}$	21(3)	21.9	79(3)	78.1
$5p_{1/2}13s_{1/2}$	23(4)	36.7	77(4)	63.3
$5p_{1/2}14s_{1/2}$	25(2)	20.1	75(2)	79.9
$5p_{1/2}15s_{1/2}$	15(2)	29.3	85(2)	70.7
$5p_{1/2}16s_{1/2}$	20(2)	21.5	80(2)	78.5
$5p_{1/2}18s_{1/2}^a$	16(3)	26.5	84(3)	73.5
$5p_{1/2}19s_{1/2}$	18(2)	33.9	82(2)	66.1
$5p_{1/2}20s_{1/2}$	22(2)	16.4	78(2)	83.6

<sup>a</sup>The  $5s17s^1S_0$  state is degenerate with the  $5s17d^1D_2$  state, and thus it is not possible to make unambiguous measurements for the Sr  $5p_{1/2}17s_{1/2}$  state.

TABLE III. The asymmetry parameters  $\beta_{5s_{1/2}}$ ,  $\beta_{4d_j}$ , and  $\beta_{5p_{1/2}}$  for Sr  $5p_{3/2}ns_{1/2}$   $J = 1$  autoionizing states.

State	Asymmetry parameters				
	$\beta_{5p_{1/2}}$		$\beta_{5s_{1/2}}$		$\beta_{4d_j}$
	Experiment	Theory	Experiment	Theory	Experiment
$5p_{3/2}10s_{1/2}$			1.75(06)	1.75	0.65(17)
$5p_{3/2}11s_{1/2}$			1.81(04)	1.75	0.64(13)
$5p_{3/2}12s_{1/2}$			a		
$5p_{3/2}13s_{1/2}$			a		
$5p_{3/2}14s_{1/2}$			a		
$5p_{3/2}15s_{1/2}$			1.78(05)	1.80	0.70(14)
$5p_{3/2}16s_{1/2}$	1.60(30)	1.56	1.78(10)	1.69	0.73(15)
$5p_{3/2}18s_{1/2}^b$	1.31(25)	1.56	1.80(04)	1.69	0.87(14)
$5p_{3/2}19s_{1/2}$	1.50(25)	1.56	1.60(08)	1.69	0.87(16)
$5p_{3/2}20s_{1/2}$	1.30(25)	1.56	1.87(06)	1.69	0.76(13)

<sup>a</sup>These  $\beta$  values vary across the state and are plotted in Figs. 6, 7, and 9.

<sup>b</sup>The  $5s17s^1S_0$  state is degenerate with  $5s17d^1D_2$  state, and thus it is not possible to make measurements of the Sr  $5p_{3/2}17s_{1/2}$  state.

TABLE IV. The branching ratio for Sr  $5p_{3/2}ns_{1/2}$   $J = 1$  autoionizing states.

State	Branching ratios to Sr <sup>+</sup> ion states (%)					
	$R_{5p_{1/2}}$		$R_{5s_{1/2}}$		$R_{4d_j}$	
	Experiment	Theory	Experiment	Theory	Experiment	Theory
$5p_{3/2}10s_{1/2}$			35(6)	46.4	65(6)	53.6
$5p_{3/2}11s_{1/2}$			34(4)	46.4	66(4)	53.6
$5p_{3/2}12s_{1/2}$			a			
$5p_{3/2}13s_{1/2}$			a			
$5p_{3/2}14s_{1/2}$			a			
$5p_{3/2}15s_{1/2}$			27(4)	31.2	73(4)	68.8
$5p_{3/2}16s_{1/2}$	7(3)	11.4	25(8)	31.2	68(8)	57.4
$5p_{3/2}18s_{1/2}^b$	8(3)	11.4	24(6)	31.2	68(6)	57.4
$5p_{3/2}19s_{1/2}$	8(3)	11.4	35(5)	31.2	57(5)	57.4
$5p_{3/2}20s_{1/2}$	7(3)	11.4	28(5)	31.2	65(5)	57.4

<sup>a</sup>Branching ratios are plotted in Figs. 6, 7, and 8.

<sup>b</sup>The  $5s17s^1S_0$  state is degenerate with  $5s17d^1D_2$  state, and thus it is not possible to make measurements of the Sr  $5p_{3/2}17s_{1/2}$  state.

tation of the  $5pns$  autoionizing states. By comparing the ratio of the signal from the  $\leq 60$ -meV electrons to the ion signal we were able to relate it to the analogous ratio of the electron signals corresponding to autoionization to the  $\text{Sr}^+ 5s_{1/2}$  and  $4d_j$  states to the ion signal, thereby determining the branching ratio for the  $\text{Sr}^+ 5p_{1/2}$  state. A second approach was to vary a dc extraction voltage applied across plates 2 and 3 to extract all the electrons. At 2 V extraction voltage all the  $\leq 60$ -meV electrons were detected, and when the extraction voltage was raised to 70 V, all the 3-eV electrons were collected as well. Thus by comparing the electron-to-ion single ratios at 2 and 70 V extraction voltages we obtained an independent value of the branching ratio to the  $\text{Sr}^+ 5p_{1/2}$  state. Although we have some concern about the effects of the field produced by the 70 V extraction voltage on the excitation, it is interesting to note that the branching ratios determined by these two methods are equal, within our experimental uncertainties.

The  $\text{Sr } 5p_{3/2}ns_{1/2} J=1$  autoionizing states for  $n > 15$  lie above  $\text{Sr}^+ 5p_{1/2}$  ionization limit, and they decay into ten continuum channels, yielding autoionization electrons of four different kinetic energies. Autoionization into the  $\text{Sr}^+ 5s_{1/2}$ ,  $5s_{1/2}\epsilon p_{1/2}$  and  $5s_{1/2}\epsilon p_{3/2}$  continua yields free electrons with a kinetic energy 2.9 eV. Decay into the  $\text{Sr}^+ 4d_{3/2}$  and  $4d_{5/2}$  continua results in two groups of  $\approx 1$ -eV electrons with a constant energy difference of 0.035 eV between them, which was not resolved in the present experiment. There are six  $4d_j$  continuum channels:  $4d_{3/2}\epsilon f_{5/2}$ ,  $4d_{5/2}\epsilon f_{7/2}$ ,  $4d_{5/2}\epsilon f_{5/2}$ ,  $4d_{3/2}\epsilon p_{1/2}$ ,  $4d_{3/2}\epsilon p_{3/2}$ , and  $4d_{5/2}\epsilon p_{3/2}$ . Decay into the  $\text{Sr}^+ 5p_{1/2}$  continuum releases electrons with kinetic energy between 50 meV for  $n=20$  and 16 meV for  $n=16$ , belonging to two continuum channels  $5p_{1/2}\epsilon s_{1/2}$  and  $5p_{1/2}\epsilon d_{3/2}$ . Due to small residual stray electric fields, such low-energy electrons did not reach the detector in the usual operating configuration, a free drift length of 18 cm. To circumvent this difficulty, the experiment was performed in the following ways. First, at a free drift length of  $L=18$  cm, we collected the electrons corresponding to  $\text{Sr}^+ 5s_{1/2}$  and  $4d_j$  ion states. We then reduced the free drift length to  $L=5$  cm, increasing the acceptance angle to  $20^\circ$ , and collected the data for the low-energy electrons corresponding to  $\text{Sr}^+ 5p_{1/2}$  ion state. For the  $5p_{3/2}16s_{1/2}$  and  $5p_{3/2}18s_{1/2}$  states, we had to apply a small bias voltage to both plates 2 and 3 in order to collect the low-energy electrons. Since both plates were biased at the same small voltage,  $\leq 0.3$  V, to first order this produced no field in the interaction region, and the net effect was to increase the acceptance angle. The asymmetry parameter for autoionization to the  $\text{Sr}^+ 5p_{1/2}$  ion core was measured this way.

The asymmetry parameters and branching ratios for the  $\text{Sr } 5p_{3/2}ns_{1/2}$  and  $5p_{1/2}ns_{1/2} J=1$  states autoionizing to the  $\text{Sr}^+ 5s_{1/2}$ ,  $4d_j$ , and  $5p_{1/2}$  ion states are listed in Table I–IV. Due to the relatively small fine-structure splitting, 0.009 eV, of the  $\text{Sr}^+ 5p_{1/2}$  and  $5p_{3/2}$  states (compare with the 0.21-eV  $\text{Ba}^+ 6p$  fine-structure splitting<sup>19</sup>) only the  $\text{Sr } 5p_{3/2}ns_{1/2}$  states for  $n > 15$  lie above the  $\text{Sr}^+ 5p_{1/2}$  limit, where they can decay to  $5p_{1/2}\epsilon s_{1/2}$  and  $5p_{1/2}\epsilon d_{3/2}$  continua. The branching-ratio measure-

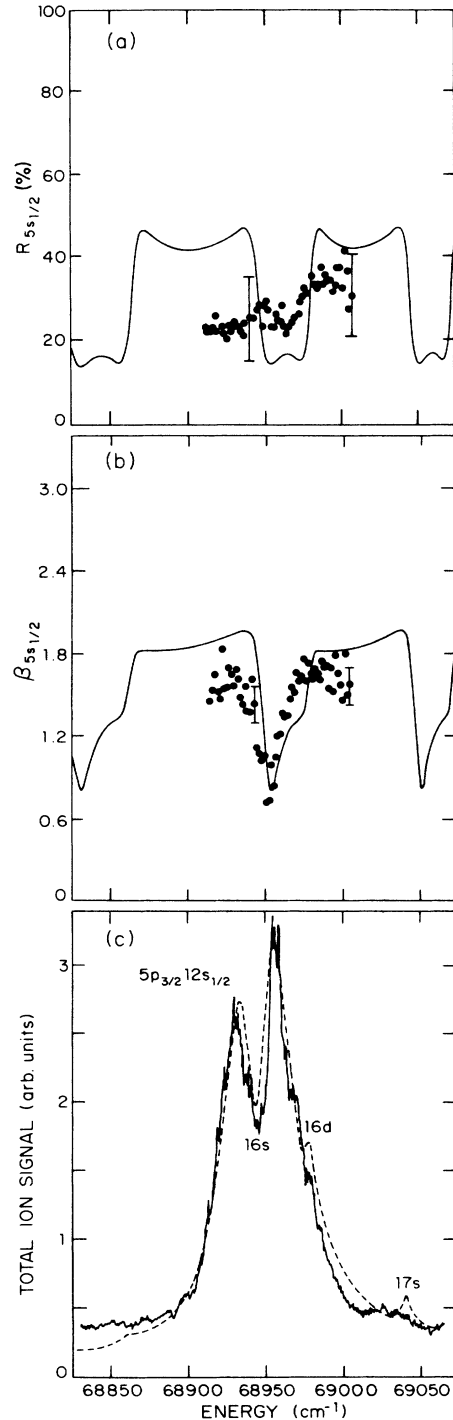


FIG. 6. (a) Branching ratio  $R_{5s_{1/2}}$  across the  $5p_{3/2}12s_{1/2}$  state, experimental data ( $\bullet$ ), the MQDT calculation (—). (b) The asymmetry parameter  $\beta_{5s_{1/2}}$  for the autoionization of the  $5p_{3/2}12s_{1/2} J=1$  state to the  $\text{Sr}^+ 5s_{1/2}$  continuum, experimental data ( $\bullet$ ), the simulation of the six-channel MQDT  $J=1$  autoionizing state showing the structure imposed by the interacting  $5p_{1/2}16s_{1/2}$  and  $5p_{1/2}16d_{3/2}$  channels, experimental data (—), the MQDT simulation (---). The structures associated with these states are labeled.

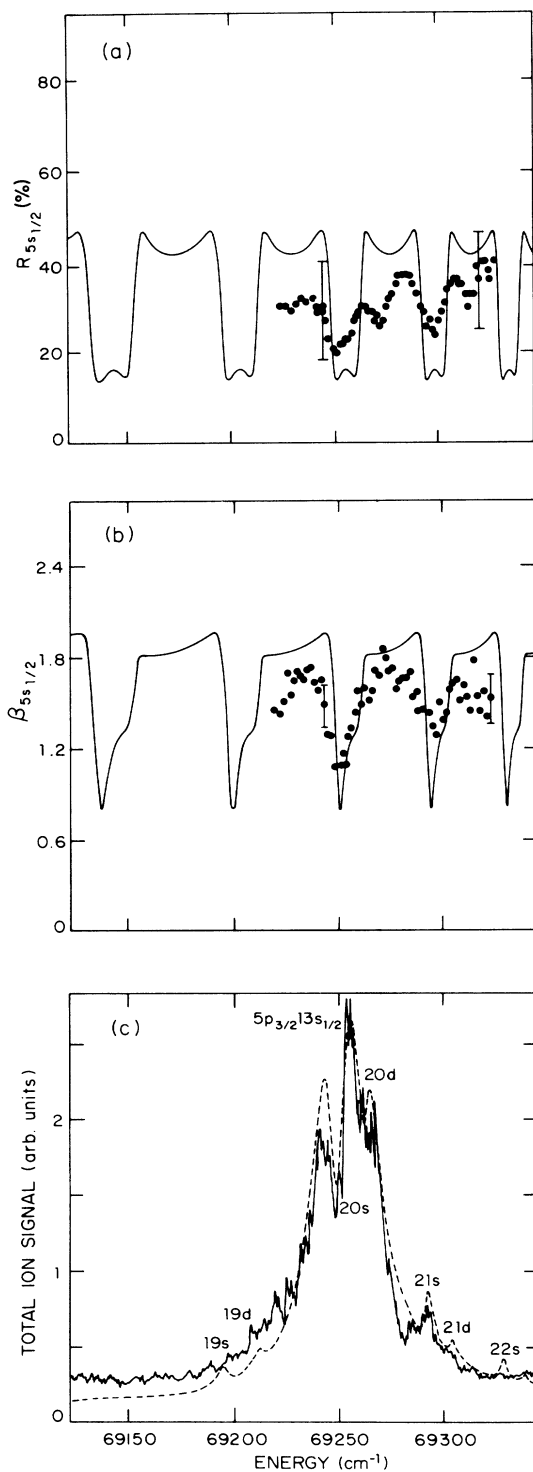


FIG. 7. (a) Branching ratio  $R_{5s_{1/2}}$  vs energy for the  $5p_{3/2}13s_{1/2} J=1$  state, experimental results ( $\bullet$ ), MQDT calculation (—). (b) The spectrum of the asymmetry parameter  $\beta_{5s_{1/2}}$  for the autoionization of the  $5p_{3/2}13s_{1/2} J=1$  state to the  $\text{Sr}^+ 5s_{1/2}$  continuum, experimental data ( $\bullet$ ), and the solid line is the MQDT fit (—). (c) The excitation spectrum of the  $5p_{3/2}13s_{1/2} J=1$  autoionizing state,  $5p_{1/2}ns_{1/2}$  and  $5p_{1/2}nd_{3/2} J=1$  states are labeled.

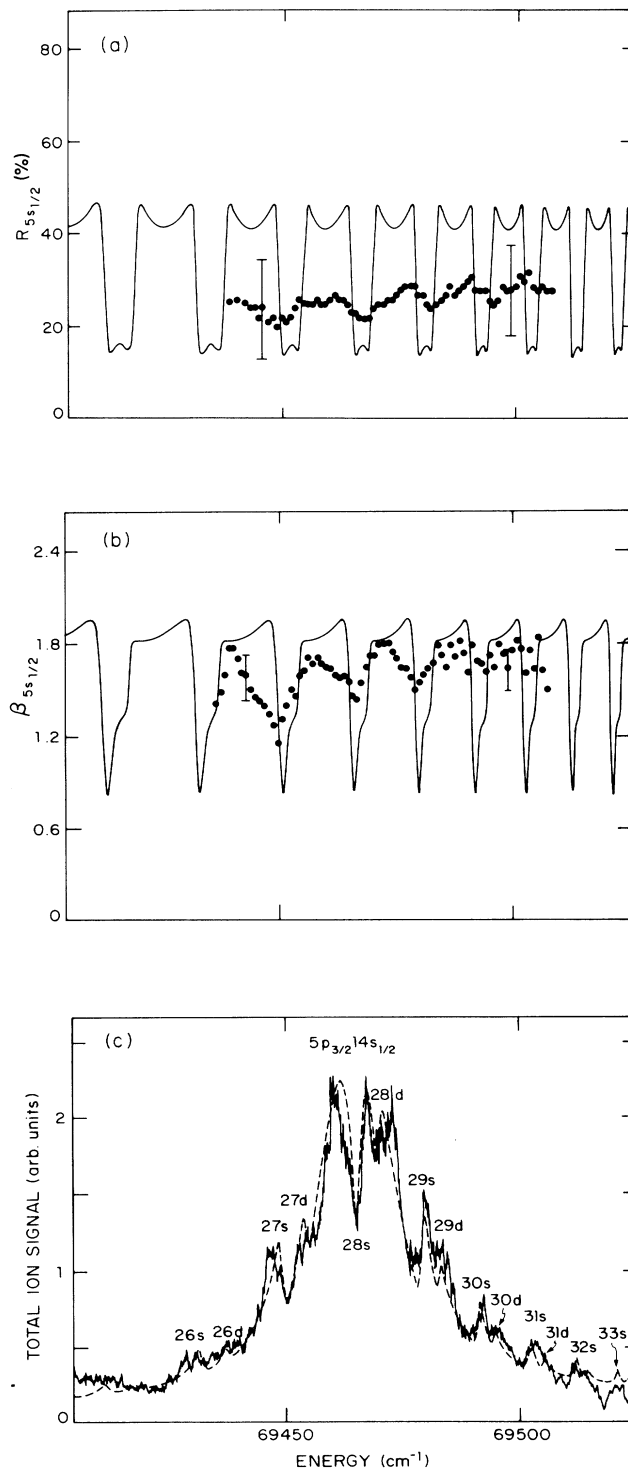


FIG. 8. (a) Experimental ( $\bullet$ ) and calculated (—) branching ratio  $R_{5s_{1/2}}$  for the  $5p_{3/2}14s_{1/2} J=1$  autoionizing state. (b) The asymmetry parameter  $\beta_{5s_{1/2}}$  across the line profile of the  $5p_{3/2}14s_{1/2} J=1$  autoionizing state, experimental data ( $\bullet$ ), MQDT simulation (—). (c) The excitation spectrum of the  $5p_{3/2}14s_{1/2} J=1$  state, experimental data (—), and the MQDT calculation (---). The structures produced by the high-lying  $5p_{1/2}ns_{1/2}$  and  $5p_{1/2}nd_{3/2}$  states are labeled.

ments show that only about 8% of Sr  $5p_{3/2}ns_{1/2}$ ,  $n > 15$ ,  $J=1$  atoms decay into the Sr<sup>+</sup>  $5p_{1/2}$  excited state with the ejected electrons of orbital angular momentum  $l=2$  or 0.

Inside the linewidths of the Sr  $5p_{3/2}12s_{1/2}$ ,  $5p_{3/2}13s_{1/2}$ , and  $5p_{3/2}14s_{1/2}$   $J=1$  autoionizing states, there are located several  $5p_{1/2}ns_{1/2}$  and  $5p_{1/2}nd_{3/2}$   $J=1$  autoionizing states. The discrete-discrete interactions of these three series produce considerable structure in the autoionization line profiles of the  $5p_{3/2}12s_{1/2}$ ,  $5p_{3/2}13s_{1/2}$ , and  $5p_{3/2}14s_{1/2}$  states. This is shown in the ion spectra of Figs. 6(c), 7(c), and 8(c). One would expect that this localized interaction should also appear in the electron spectra. In fact this is the case, and in Figs. 6(b), 7(b), and 8(b), we present the asymmetry parameter  $\beta_{5s_{1/2}}$  for the autoionization of these three states to the Sr<sup>+</sup>  $5s_{1/2}$  ion state plotted as a function of the energy. The same interaction also affects the angular distributions of the electrons ejected from the interacting  $5p_{1/2}ns_{1/2}$   $J=1$  states. As shown in Table I, the  $5p_{1/2}16s_{1/2}$ , and  $5p_{1/2}20s_{1/2}$   $J=1$  states are the most affected. This is hardly surprising since these two states are located at the centers of the  $5p_{3/2}12s_{1/2}$  and  $5p_{3/2}13s_{1/2}$   $J=1$  states, respectively [see Figs. 6(c) and 7(c)]. The only observed variation in asymmetry parameter occurs in  $\beta_{5s_{1/2}}$ . Within our experimental uncertainty,  $\beta_{4d_j}$  does not change noticeably. This is not surprising since the  $4d_j$  ion cores can share the asymmetry with the ejected electron, and there are many channels to average out the changes in  $\beta_{4d_j}$ . Although there is no observable change in  $\beta_{4d_j}$ , the branching ratios between Sr<sup>+</sup>  $5s_{1/2}$  and  $4d_j$  states do vary across the line profiles as shown in Figs. 6(a), 7(a), and 8(a), but the experimental uncertainties are comparable to the observed variations.

#### IV. THEORY

##### A. Introduction

The general angular properties of photoelectron angular distributions have been worked out by Fano and Dill using the concept of angular-momentum transfer.<sup>20,21</sup> Here we use this general framework and calculate the specific matrix elements we need using an extension of the MQDT formulation of Cooke and Cromer,<sup>8</sup> which is quite similar to the formulation of Giusti-Suzor and Fano.<sup>9</sup> There are two attractive features to this approach. First, the angular-momentum-transfer approach enables us to easily draw some general conclusions, which are not so transparent using other approaches. Second, the Cooke and Cromer approach to MQDT describes autoionizing states in terms of coupling to a small number of interacting continua which are unspecified linear combinations of the available continua. This approach provides a set of parameters which matches in a very direct way the total excitation spectra using the isolated core-excitation approach. In fact the total photoexcitation spectra of the Sr  $5pns$  states have already been analyzed using a six-channel quantum-

defect-theory model,<sup>17</sup> and we shall use this analysis as the starting point of our MQDT treatment.

By measuring the energy and angular distributions of the ejected electrons we specify the interacting continua in terms of the well-defined  $(J_{cs}, l)$  continua. We specify the continua not in the more familiar  $LS$  or  $jj$  representations but in a  $J_{cs}, l$  representation, where  $J_{cs}$  is the total angular momentum of the ion core and the ejected electron's spin, and  $l$  is the ejected electron's angular momentum. In practice, the specification corresponds to identifying the elements of a unitary matrix  $U$  relating the interacting and  $(J_{cs}, l)$  continua. Thus the theoretical task in the present work is to augment the already-existing MQDT parameters by determining  $U$  matrix elements.

We note that our approach is similar to that used by Kachru *et al.*,<sup>15</sup> but there are two important differences. In that work the angular-momentum-transfer approach was not used, and the Lee and Lu<sup>22</sup> formulation of quantum-defect theory was used to calculate the matrix elements. With this in mind, in this section we only briefly summarize the relevant results of the angular-momentum-transfer approach. We then describe the calculation of the matrix elements using quantum-defect theory, and finally, apply the results to the Sr  $5pns$  states.

##### B. General angular properties

The essence of the angular-momentum-transfer method, as applied to photoelectron spectroscopy, is that the angular distribution of the ejected electrons can be expressed as a sum of incoherent contributions corresponding to different magnitudes of the angular momentum transferred to an unpolarized target. The asymmetry parameter  $\beta$  can be conveniently expressed as the weighted average of the contributions from the parity-favored and parity-unfavored transitions, respectively.

Consider the schematic ionization process

$$\text{Sr}(\mathbf{J}_0, \pi_0) + \gamma(\mathbf{J}_\gamma, \pi_\gamma) \rightarrow \text{Sr}^+(\mathbf{J}_c, \pi_c) + e^-(l, s, \pi_e = (-1)^l). \quad (2)$$

Here Sr is the initially unpolarized excited  $5sns \ ^1S_0$  Sr atom;  $\mathbf{J}_0$  and  $\pi_0$  refer to its angular momentum and parity, respectively;  $\gamma$  is the incident photon,  $\mathbf{J}_\gamma$  and  $\pi_\gamma$  represent its angular momentum and parity; Sr<sup>+</sup> is the residual ion resulting from the photoionization;  $\mathbf{J}_c$  and  $\pi_c$  indicate its angular momentum and parity. Angular-momentum conservation and parity conservation require that

$$\mathbf{J} = \mathbf{J}_0 + \mathbf{J}_\gamma = \mathbf{J}_c + \mathbf{S} + l = \mathbf{J}_{cs} + l, \quad (3)$$

$$\Pi = \pi_0 \pi_\gamma = \pi_c (-1)^l. \quad (4)$$

Here  $\mathbf{J}$  is the total angular momentum. The electron spin  $\mathbf{S}$  is coupled to the angular momentum of the ion to form a resultant angular momentum  $\mathbf{J}_{cs}$ , which we do not observe. The angular momentum transferred to the unobserved ion core and electron spin in the process is

$$\mathbf{J}_t = \mathbf{J}_{cs} - \mathbf{J}_0 = \mathbf{J}_\gamma - l. \quad (5)$$

The allowed  $J_t$  values are determined from Eq. (5). Values of  $J_t$  are parity favored if  $\pi_0 \pi_c = (-1)^{J_t}$  and un-

avored if  $\pi_0\pi_c = -(-1)^{J_t}$ . As a general rule, parity-favored processes are those which require no spin reorientation while parity-unfavored processes do. The photoionization cross section to a given ion-core state  $c$  is<sup>20,21</sup>

$$\sigma_c = \sum_{J_t} \sigma_c(J_t), \quad (6)$$

and the asymmetry parameter  $\beta_c$  is given by the weighted average of the asymmetry parameters

$$\beta_c = \frac{\left[ \sum_{J_t}^{\text{fav}} \sigma_c(J_t) \beta_c(J_t) - \sum_{J_t}^{\text{unf}} \sigma_c(J_t) \right]}{\left[ \sum_{J_t} \sigma_c(J_t) \right]}. \quad (7)$$

For a parity-favored process,  $\beta_c$  is given by

$$[\beta_c(J_t)]_{\text{fav}} = \frac{\{(J_t+2) |S_+(J_t)|^2 + (J_t-1) |S_-(J_t)|^2 - 3J_t(J_t+1)^{1/2} [S_+(J_t)S_-^\dagger(J_t) + S_+^\dagger(J_t)S_-(J_t)]\}}{(2J_t+1)(|S_+(J_t)|^2 + |S_-(J_t)|^2)}. \quad (10)$$

Here  $S_\pm(J_t)$  denotes the modified reduced scattering matrix element  $S_l(J_t)$  for a given  $J_t$  and  $l=J_t\pm 1$ . It is related to the reduced scattering matrix element expressed in terms of  $J$  by the following equality:

$$S_l(J_t) = \sum_{J_t} (-1)^{J_0-J-J_t} (2J+1) \begin{Bmatrix} l & J_{cs} & J \\ J_0 & J_\gamma & J_t \end{Bmatrix} \times \langle (J_c S) J_{cs} l | S(J) | J_0 J_\gamma \rangle, \quad (11)$$

where the braces indicate a Wigner 6- $J$  symbol. In writing the reduced scattering matrix element we have dropped the subscript  $c$  for simplicity of notation. However, in all scattering matrix elements such as the ones of Eqs. (10) and (11) the specification of the ion-core state is implicit (it obviously makes no sense to speak of the  $\beta$  parameter without specifying the ion core).

The partial cross section corresponding to the parity-favored transition is

$$[\sigma_c(J_t)]_{\text{fav}} = \lambda^2 \frac{2J_c+1}{4\pi(2J_0+1)} \left[ |S_+(J_t)|^2 + |S_-(J_t)|^2 \right]. \quad (12)$$

Here  $\lambda$  is the wavelength of the incident photon, and  $S_\pm(J_t)$  is defined below Eq. (10). For parity-unfavored transitions the corresponding cross section is

$$[\sigma_c(J_t)]_{\text{unf}} = \lambda^2 \frac{2J_t+1}{4\pi(2J_0+1)} |S_0(J_t)|^2. \quad (13)$$

Here  $S_0(J_t)$  is the modified reduced scattering matrix element for the value of  $J_t=l$ .  $S_l(J_t)$  may be expressed in terms of a sum of reduced electric dipole matrix elements  $D$  as

In writing Eq. (7) we have taken advantage of the fact that  $\beta_c \equiv -1$  for a parity-unfavored process. The total photoionization cross section is given by the sum of the cross sections to the ion-core states

$$\sigma_T = \sum_c \sigma_c, \quad (8)$$

and the branching ratio  $R_c$  for autoionization to a particular ion-core state  $c$ , and the ejection of electrons with the commensurate kinetic energy, is given by

$$R_c = \frac{\sigma_c}{\sigma_T}. \quad (9)$$

$$S_l(J_t) = \left[ \frac{4\pi\alpha\hbar\omega^3}{3c^2} \right]^{1/2} (-1)^{J_0-J-1} (2J+1)^{1/2} \times \begin{Bmatrix} J_{cs} & l & J \\ 1 & J_0 & J_t \end{Bmatrix} \langle (J_c S) J_{cs}, l, J - \| D \| J_0 \rangle. \quad (14)$$

Here  $\alpha$  is the fine-structure constant, and the minus sign in the reduced matrix element indicates that the final state is normalized according to incoming-wave boundary conditions.

### C. Evaluation of the matrix elements by quantum-defect theory

In this section we develop an expression for the reduced matrix element of Eq. (14) for the specific case of the  $5p_j ns_{1/2}$  states.

Below the  $\text{Sr}^+ 5p_{1/2}$  limit there are eight  $J=1$  odd-parity continua. It is useful to first specify them in the  $jj$  representation. In  $jj$  coupling they are  $5s_{1/2} \epsilon p_{1/2}$ ,  $5s_{1/2} \epsilon p_{3/2}$ ,  $4d_{3/2} \epsilon p_{1/2}$ ,  $4d_{3/2} \epsilon p_{3/2}$ ,  $4d_{3/2} \epsilon f_{5/2}$ ,  $4d_{5/2} \epsilon p_{3/2}$ ,  $4d_{5/2} \epsilon f_{5/2}$ , and  $4d_{5/2} \epsilon f_{7/2}$ . The  $5p_{1/2} ns_{1/2}$ ,  $5p_{1/2} nd_{3/2}$ , and  $5p_{3/2} ns_{1/2}$  series interact with all of them to some extent. The interactions with the continua may, however, be represented by the interaction with only three continua,  $\psi_1^c$ ,  $\psi_2^c$ , and  $\psi_3^c$ , which are linear combinations of the above continua.

This representation of the continua is adequate for the total excitation spectra obtained by the ICE method, which tells us nothing more about the continua than that they act as a sink for electrons. Accordingly the total excitation spectra of the  $\text{Sr } 5pns$   $J=1$  series have recently been analyzed using a six-channel model. The six  $J=1$  channels are

$\phi_1$	$\phi_2$	$\phi_3$	$\phi_4$	$\phi_5$	$\phi_6$
$5p_{3/2}ns_{1/2}$	$5p_{1/2}ns_{1/2}$	$5p_{1/2}nd_{3/2}$	$\psi_1^c$	$\psi_2^c$	$\psi_3^c$

Above the  $5p_{1/2}$  limit channels  $\phi_2$  and  $\phi_3$  become continua as well, and in this region we label them as  $\psi_4^c$  and  $\psi_5^c$  for consistency.

The wave function is a combination of the collision channel wave functions which is determined by solving the matrix equation

$$(\epsilon + R)a = 0 \quad (15)$$

at each energy. Here  $\epsilon$  is a diagonal matrix with entries  $\epsilon_{ii} = \tan\pi(\nu_i + \mu_i)$  for closed channels, where  $\nu_i$  is an effective quantum number and  $\mu_i$  is a quantum defect. For open channels  $\epsilon_{ii} = \tan\tau$ .  $R$  is a symmetric, off-diagonal matrix specifying the interchannel couplings,  $a_i = Z_i \cos[\pi(\nu_i + \mu_i)]$  for a closed channel, and  $a_i = Z_i \cos\tau$  for an open channel. For the nontrivial solution,  $a \neq 0$ , Eq. (16) leads to an equation for  $\tau$  with the number of roots equal to the number of open collision channels. Below the  $5p_{1/2}$  limit there are three roots, and above there are five. The roots are radial eigenphase shifts  $\tau_\rho$ , which are differentiated by the subscript  $\rho$  (the phases of the radial wave functions are measured relative to hydrogenic wave functions). Each  $\tau_\rho$  value leads to a set of  $Z_{i\rho}$  values which determine an independent wave function. Explicitly, it is given by

$$\Phi_\rho = \sum_i Z_{i\rho} \phi_i, \quad (16)$$

where the normalization condition

$$\sum_i Z_{i\rho}^2 = 1$$

is applied, the sum on  $i$  running over the open channels. In all summations that follow the summation over all values of the indices specified below the summation sign is implied.

By adjusting the values of  $\mu_i$  and  $R_{ij}$ , which are energy independent, to fit the positions and widths of the autoionizing states, the correct variation of  $Z_{i\rho}$  with energy for all open and closed channels is determined.

As stated in the previous paper,<sup>17</sup> the three continuum channels may be chosen to be orthogonal so that  $R_{45} = R_{46} = R_{56} = 0$ , and channels 2 and 3, which converge to the same limit, are found experimentally to be orthogonal to each other, so that  $R_{23} = 0$ . To reduce the number of channel-interaction parameters further, we constrain the model by requiring channel 1 to decay to continuum  $\psi_1^c$ , channel 2 to continuum  $\psi_2^c$ , and channel 3 to continuum  $\psi_3^c$ . In other words, we require that  $R_{15} = R_{16} = R_{24} = R_{34} = R_{35} = 0$ . Although this requirement is apparently arbitrary, there is a justification. Four- and five-channel analyses of the  $5pns$  series with three bound channels and one or two continuum channels are significantly inferior to the six-channel model, indicating that bound channels do decay in appreciable measure to different continua. That orthogonal bound states decay in a large part to orthogonal continua is not entirely unexpected, and it has been repeatedly

confirmed in the MQDT analyses of Ba and Sr autoionizing series.<sup>12,13,23</sup> Recently it has led to the possibility of controlled autoionization to a specific  $Ba^+$  ion state by the excitation of satellite features in the spectra.<sup>24</sup> In Table V we tabulate the MQDT parameters for the Sr  $5pns$  states obtained from analyses of the total photoexcitation spectra. As we have mentioned, these values of  $\mu_i$  and  $R_{ij}$  determine the values of  $Z_{i\rho}$  and hence the wave function. From Eq. (16) it is apparent that each eigenchannel wave function has both closed and open parts. For simplicity we will from now on denote open and closed collision channels by the subscripts  $i$  and  $j$ , respectively. While the values of  $Z_{i\rho}$  are of no direct consequence in the evaluation of total photoexcitation spectra, which are only sensitive to  $Z_{j\rho}$  values, they are critical to the electron spectroscopy. In essence when we excite an autoionizing state we excite the closed  $Z_{j\rho}$  part of the  $\rho$  eigenchannel wave function which decays into the open  $Z_{i\rho}$  part.

#### D. Below the $5p_{1/2}$ limit

At this point we have only to relate the three interacting  $\psi_i^c$  channels to the eight open channels below the  $5p_{1/2}$  limit. We choose to express them as  $J_{cs}l$  channels because we do not observe the angular properties of either the ion core or the electron spin. We note that for the  $5sep$  continua the  $J_{cs}l$  and LS continua are the same, i.e.,  $J_{cs} = 1$  corresponds to  $^3P_1$  and  $J_{cs} = 0$  corresponds to  $^1P_1$ . The three interacting continuum channels  $\psi_i^c$  must be linear combinations of the above eight  $J_{cs}l$  continuum channels. Similarly there are five noninteracting channels  $\psi_i^n$ , and in general there is a unitary transformation matrix  $U$  such that

$$\begin{pmatrix} \psi_1^c \\ \psi_2^c \\ \psi_3^c \\ \psi_4^n \\ \psi_5^n \\ \psi_6^n \\ \psi_7^n \\ \psi_8^n \end{pmatrix} = U \begin{pmatrix} \phi_{5s_{1/2}(0,1)} \\ \phi_{5s_{1/2}(1,1)} \\ \phi_{4d_{3/2}(1,1)} \\ \phi_{4d_{3/2}(2,1)} \\ \phi_{4d_{3/2}(2,3)} \\ \phi_{4d_{5/2}(2,1)} \\ \phi_{4d_{5/2}(2,3)} \\ \phi_{4d_{5/2}(3,3)} \end{pmatrix}, \quad (17)$$

where the numbers in parentheses are  $J_{cs}$  and  $l$ , i.e., (0,1) is  $J_{cs} = 0$  and  $l = 1$ .

TABLE V. MQDT parameters.

$\mu_1 = 3.441^{a,b}$	$R_{12} = 0.16^b$	$U_{11} = 0.570$
$\mu_2 = 3.410$	$R_{13} = 0.10$	$U_{12} = 0.158$
$\mu_3 = 2.100$	$R_{14} = 0.45$	$U_{21} = 0.470$
	$R_{25} = 0.40$	$U_{22} = -0.170$
	$R_{36} = 0.39$	$U_{31} = 0.547$
		$U_{32} = 0.028$

<sup>a</sup>The quantum defects are only known modulo 1.

<sup>b</sup>Reference 17.

We can now express the matrix element of Eq. (14) as  $\langle (J_c S) J_{cs} l, J - \| D \| J_0 \rangle$

$$= \sum_{\rho, i} U_{ik} Z_{i\rho} Z_{j\rho} \langle \phi_j \| D \| J_0 \rangle e^{i\tau_\rho} e^{i\sigma_{J_c, l}}, \quad (18)$$

where the subscript  $k$  refers to a specific  $|(J_c S) J_{cs} l, J - \rangle$  continuum channel. In this expression the summation on  $\rho$  runs over the three eigenchannels of our six-channel model, and the summation on  $i$  runs over the three open collision channels. In writing Eq. (18) we have assumed the usual situation of ICE, that there is excitation into only one closed channel,  $j=1$  for  $5p_{3/2}ns_{1/2}$  states or  $j=2$  for  $5p_{1/2}ns_{1/2}$  states. For cases in which more than one closed channel is excited, it is straightforward to generalize Eq. (18) by summing over  $j$ . In Eq. (18) the phase factor  $e^{i\tau_\rho}$  reflects the change from incoming-wave normalization to standing wave normalization.  $\sigma_{J_c, l}$  is the Coulomb phase for an electron of angular momentum  $l$  leaving an ion core of angular momentum  $J_c$ ,

$$\sigma_{J_c, l} = \arg \Gamma(l + 1 - iW^{-1/2}). \quad (19)$$

Here  $W$  is the kinetic energy (in atomic units) of the ejected electrons. Reading Eq. (18) from  $\langle \phi_j \| D \| J_0 \rangle$  to the left,  $\langle \phi_j \| D \| J_0 \rangle$ , or  $D_j$  represents the reduced dipole matrix element connecting the initial bound  $5sns^1S_0$  state to the  $j$  channel.  $Z_{j\rho}$  tells us how much of this  $j$  channel is in the  $\rho$  eigenchannel, and  $Z_{i\rho}$  tells us how much of the  $\rho$  eigenchannel decays into each  $\psi_i^c$  channel. Finally,  $U_{ik}$  gives us the composition of the  $\psi_i^c$  channels in terms of the  $(J_c, l)$  channels. It is important to remember that the only unknown parameters in Eq. (17) are the  $U_{ik}$  matrix elements.

When the Sr  $5p_{3/2}ns_{1/2}$  and  $5p_{1/2}ns_{1/2}$  states below the  $5p_{1/2}$  limit are excited, the ion core may be left either in the  $4d_j$  states or in the  $5s_{1/2}$  state, and the branching ratio between these two possibilities is one of the measured parameters. Additionally, the angular distributions ( $\beta$  parameters) of the ejected electrons are measured. Of these only the  $\beta$  parameter for autoionization to the  $\text{Sr}^+ 5s_{1/2}$  state can be compared to theory in a detailed way.

Let us begin with autoionization to the  $\text{Sr}^+ 5s_{1/2}$  state. In this case  $J_0=0$ ,  $J_c=\frac{1}{2}$ ,  $l=1$ ,  $J=1$ , and

$$J_t = J_{cs} = \begin{cases} 0, & \text{parity favored} \\ 1, & \text{parity unfavored} \end{cases}$$

From Eqs. (7) and (6) it is straightforward to obtain

$$\beta_{5s_{1/2}} = \frac{2 |S_1(0)|^2 - 3 |S_1(1)|^2}{|S_1(0)|^2 + 3 |S_1(1)|^2} \quad (20)$$

and

$$\sigma_{5s_{1/2}} = \frac{\lambda^2}{4\pi} (|S_1(0)|^2 + 3 |S_1(1)|^2). \quad (21)$$

For a  $5p_{3/2}ns_{1/2}$  state the  $S$  matrix elements of Eq. (14) are given by

$$S_1(0) = \left[ \frac{4\pi\alpha\hbar\omega^3}{3c^2} \right]^{1/2} i^{-1} e^{i\sigma_{1/2,1}} \langle \phi_1 \| D \| J_0 \rangle \times \sum_{\rho, i} e^{i\tau_\rho} Z_{1\rho} Z_{i\rho} U_{i1}, \quad (22)$$

$$S_1(1) = - \left[ \frac{4\pi\alpha\hbar\omega^3}{9c^2} \right]^{1/2} i^{-1} e^{i\sigma_{1/2,1}} \langle \phi_1 \| D \| J_0 \rangle \times \sum_{\rho, i} e^{i\tau_\rho} Z_{1\rho} Z_{i\rho} U_{i2}. \quad (23)$$

Using Eqs. (22) and (23) and removing the common factors from  $S_1(0)$  and  $S_2(0)$  allows us to write Eq. (20) as

$$\beta_{5s_{1/2}} = \frac{2 \left| \sum_{\rho, i} e^{i\tau_\rho} Z_{1\rho} Z_{i\rho} U_{i1} \right|^2 - \left| \sum_{\rho, i} e^{i\tau_\rho} Z_{1\rho} Z_{i\rho} U_{i2} \right|^2}{\left| \sum_{\rho, i} e^{i\tau_\rho} Z_{1\rho} Z_{i\rho} U_{i2} \right|^2 + \left| \sum_{\rho, i} e^{i\tau_\rho} Z_{1\rho} Z_{i\rho} U_{i1} \right|^2}. \quad (24)$$

Using Eqs. (9), (22), and (23), we may evaluate the branching ratio to the  $5s_{1/2}$  state of  $\text{Sr}^+$  as

$$R_{5s_{1/2}} = \frac{\left| \sum_{\rho, i} e^{i\tau_\rho} U_{i1} Z_{\rho i} Z_{\rho 1} \right|^2 + \left| \sum_{\rho, i} e^{i\tau_\rho} U_{i2} Z_{i\rho} Z_{\rho 1} \right|^2}{\sum_{\rho} Z_{\rho 1}^2}. \quad (25)$$

The  $\beta$  parameter, branching ratio, and cross section for excitation of a  $5p_{1/2}ns_{1/2}$  state are obtained by replacing  $\langle \phi_1 \| D \| J_0 \rangle$  by  $\langle \phi_2 \| D \| J_0 \rangle$  and  $Z_{1\rho}$  by  $Z_{2\rho}$  in Eqs. (22)–(24).

We begin to fit the data by examining the results of the six-channel MQDT analysis. In Fig. 9(a) we show the three eigenphases in the vicinity of the  $5p_{1/2}11s_{1/2}$ ,  $5p_{1/2}11d_{3/2}$ , and  $5p_{3/2}10s_{1/2}$  states. If we focus on the  $5p_{1/2}11s_{1/2}$  state, it is evident that most of the change in the phase occurs in the  $\rho=2$  channel. Thus the  $5p_{1/2}11s_{1/2}$  state is largely contained in this channel, and the magnitude of  $Z_{2\rho}$  is largest for  $\rho=2$  as shown by Fig. 9(b). Thus the excitation of the  $5p_{1/2}11s_{1/2}$  state occurs primarily into the  $\rho=2$  eigenchannel. Therefore we now examine the  $\phi_i$  continua which compose the  $\rho=2$  channel. In Fig. 9(c) we show the values of  $Z_{i2}$ , and, as shown, the major constituent is  $\phi_5$  (or  $\psi_5^c$ ). This is hardly unexpected since the  $R_{25}$  matrix element describes the direct autoionization of a  $5p_{1/2}ns_{1/2}$  state. In sum, for isolated  $5pns$  states below the  $5p_{1/2}$  limit, to a good approximation the  $5p_{1/2}ns_{1/2}$  and  $5p_{3/2}ns_{1/2}$  states autoionize via a single  $\rho$  eigenchannel to the  $\psi_5$  ( $\psi_5^c$ ) and  $\psi_4$  ( $\psi_4^c$ ) continua, respectively. Making this approximation simplifies the summations for the matrix elements of Eq. (18) to a single term. Thus branching ratio expressions, such as the one given by Eq. (25), reduce to sums of squared  $U$  matrix elements. From the observed branching ratios of the  $5p_{1/2}ns_{1/2}$  states we find

$$R_{5s_{1/2}} = \sum_{k=1}^2 |U_{2k}|^2 \simeq 0.25,$$

and

$$R_{4d_j} = \sum_{k=3}^8 |U_{2k}|^2 \simeq 0.75.$$

Similarly the branching ratios of the  $5p_{3/2}ns_{1/2}$  states lead to

$$R_{5s_{1/2}} = \sum_{k=1}^2 |U_{1k}|^2 \simeq 0.3,$$

and

$$R_{4d_j} = \sum_{k=3}^8 |U_{1k}|^2 \simeq 0.7.$$

The same sort of simplification occurs in the asymmetry parameters. With contributions from only one  $\rho$  and  $i$  channel, Eq. (24) for the  $5p_{3/2}ns_{1/2}$  states may be written as

$$\beta_{5s_{1/2}} = \frac{2U_{11}^2 - U_{12}^2}{U_{11}^2 + U_{12}^2}. \quad (26)$$

An analogous expression may be written for the  $5p_{1/2}ns_{1/2}$  states by replacing  $U_{11}$  and  $U_{12}$  by  $U_{21}$  and  $U_{22}$ , respectively. These expressions for  $\beta_{5s_{1/2}}$  clearly

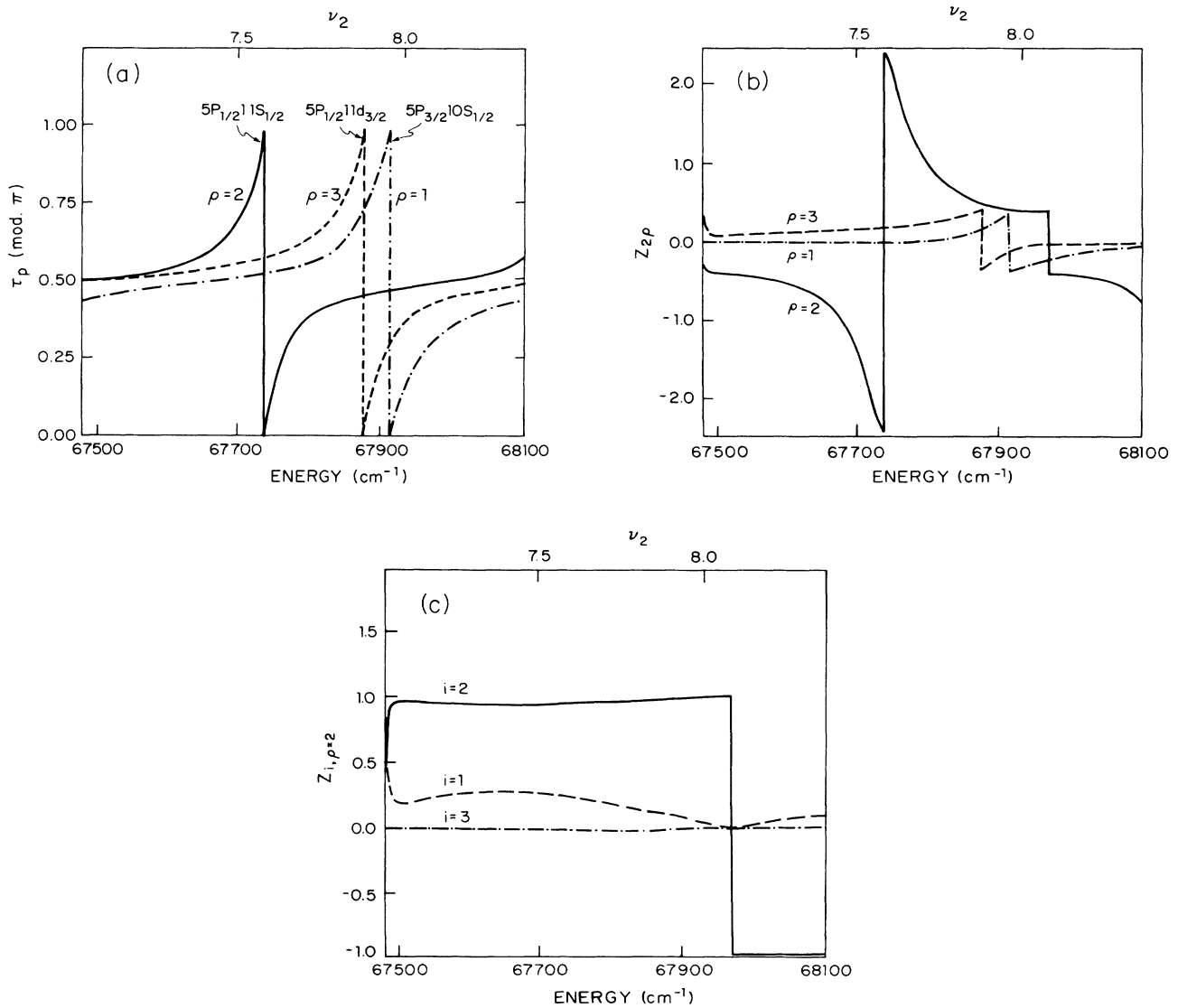


FIG. 9. (a) Three eigenphases,  $\tau_\rho$ , in the vicinity of the  $5p_{1/2}11s_{1/2}$ ,  $5p_{1/2}11d_{3/2}$ , and  $5p_{3/2}10s_{1/2}$  states. Note the phase shifts in one  $\rho$  channel at the locations of each autoionizing state. (b)  $Z_{2,\rho}$ , the coefficient of the  $5p_{1/2}ns_{1/2}$  channel in each eigenchannel. Note that only  $Z_{22}$  is very different from zero, indicating that the  $5p_{1/2}11s_{1/2}$  state is found almost exclusively in the  $\rho=2$  channel. (c) The open channel  $Z_{i,\rho}$  values for  $\rho=2$  showing that the  $i=2$  channel is by far dominant at the energy of the  $5p_{1/2}11s_{1/2}$  state.

specify the values of  $(U_{11}/U_{12})^2$  and  $(U_{21}/U_{22})^2$ . If we use for the  $5p_{3/2}ns_{1/2}$  and  $5p_{1/2}ns_{1/2}$  states values of 1.8 and 1.6 for  $\beta_{5s_{1/2}}$  we obtain values of  $(U_{11}/U_{12})^2=14$  and  $(U_{21}/U_{22})^2=6.5$ . These values together with the constraints imposed by the branching ratios allow us to determine the magnitudes of these entries of the  $U$  matrix, specifically  $U_{11}^2=0.28$ ,  $U_{12}^2=0.02$ ,  $U_{21}^2=0.21$ , and  $U_{22}^2=0.036$ . Note that we are unable to determine the signs on the basis of these data alone.

The above expressions for the branching ratio and asymmetry parameter, Eq. (26), are of course rigorously true when there is only one  $\psi_i^c$  channel and thus one

eigenchannel, as is the case above the  $5p_{1/2}$  limit. It is important to note that in this case both  $R_c$  and  $\beta_c$  can be expressed in terms of  $U$  matrix elements, which are constant and do not vary across the autoionizing state. Thus  $R_c$  and  $\beta_c$  do not vary across the autoionizing state. For practical purposes this is also true even in the case of isolated states, such as the  $5p_{1/2}11s_{1/2}$  state which is found primarily in the  $\rho=2$  channel, as shown by Fig. 9(b). To an excellent approximation  $R_{5s_{1/2}}$  and  $\beta_{5s_{1/2}}$  are constant across the  $5p_{1/2}11s_{1/2}$  state as shown by Fig. 11.

In obtaining our initial values for the  $U$  matrix ele-

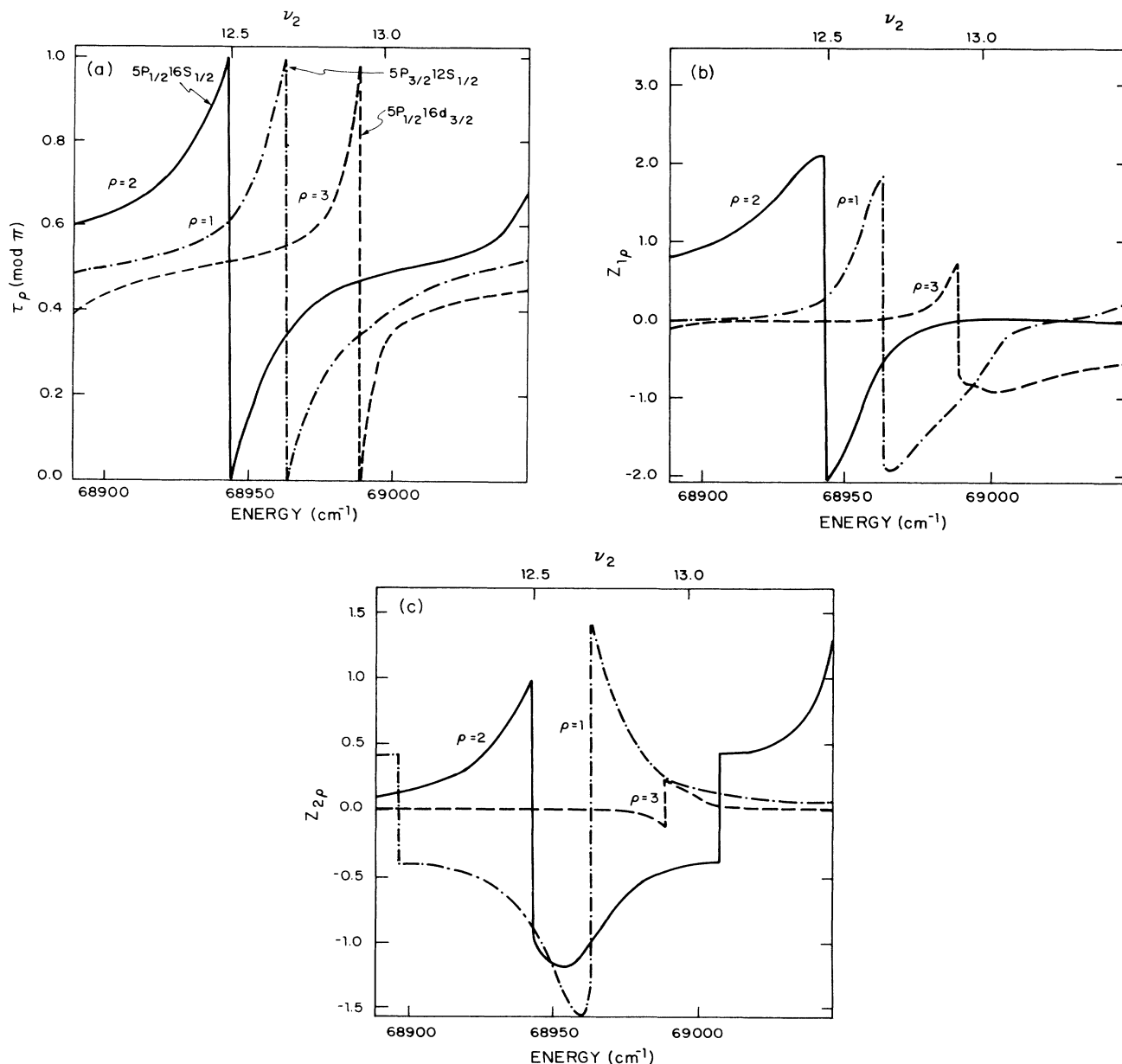


FIG. 10. (a) Eigenphases near the location of the  $5p_{3/2}12s_{1/2}$  state. (b) Variation of  $Z_{1\rho}$ , the amount of  $5p_{3/2}ns_{1/2}$  channel in each  $\rho$  channel. Note that there is significant amounts in both  $\rho=1$  and 2 channels introducing the possibility of interference. (c) Variation of  $Z_{2\rho}$ , the amount of  $5p_{1/2}ns_{1/2}$  channel. Again there is a significant contribution from two  $\rho$  channels.

ments we have chosen regions below the  $5p_{1/2}$  limit where the  $5p_{3/2}ns_{1/2}$  and  $5p_{1/2}ns_{1/2}$  states are isolated and do not exhibit channel interaction. The final determination of the  $U$  matrix elements is made by fitting the  $5pns$  states which show obvious channel interaction. In these cases there is more than one important  $\rho$  channel, and there can be quite evident variation in both the asymmetry parameter and the branching ratios across an autoionizing line profile. As a specific example of this we show in Fig. 10(a) the variation of the three eigenphases across the  $5p_{3/2}12s_{1/2}$  state, which is nearly degenerate with the  $5p_{1/2}16s_{1/2}$  state. As shown by Fig. 10(a) there are two  $\rho$  channels with significant phase shifts and therefore closed channel components. As shown by Figs. 10(b) and 10(c) there are significant amounts of the  $5p_{1/2}16s_{1/2}$  and  $5p_{3/2}12s_{1/2}$  states, as shown by  $Z_{2\rho}$  and  $Z_{1\rho}$ , in both  $\rho=1$  and 2 channels. Thus both  $\rho$  channels are important in determining the branching ratios, and asymmetry parameters and the phase variation becomes important for both the  $5p_{1/2}16s_{1/2}$  and  $5p_{3/2}12s_{1/2}$  states. The calculated and observed variation in the  $R_{5s_{1/2}}$  in the excitation of the  $5p_{3/2}12s$  state is shown in Fig. 6. The calculated variation of  $\beta_{5s_{1/2}}$  and  $R_{5s_{1/2}}$  for the  $5p_{1/2}ns_{1/2}$  states is shown in Fig. 11. The decrease in  $\beta_{5s_{1/2}}$  and  $R_{5s_{1/2}}$ , seen in Fig. 11, coincide with the locations of the  $5p_{3/2}ns_{1/2}$  states. The variations with energy is slow enough that across any  $5p_{1/2}ns_{1/2}$  state it is not readily observable. However, along the  $5p_{3/2}ns_{1/2}$  series it clearly is.

The observed variations in  $\beta_{5s_{1/2}}$  with energy shown in Figs. 6–8 are used to refine our initial values of the  $U$  matrix elements. Since we have already determined their magnitudes fairly well, the most important results of this are the relative signs. The  $U$  matrix values used to calculate the curves of Figs. 6–8 and 11 are given in Table V. It is useful to write out  $\psi_i^c$  channels in terms of the  $(J_{cs}l)$  channels. They are

$$\begin{aligned} \psi_1^c = & 0.57 |5s_{1/2}(0,1)\rangle + 0.16 |5s_{1/2}(1,1)\rangle \\ & + \sum_{k=3}^8 U_{1k} |4d\epsilon l\rangle, \end{aligned}$$

where

$$\sum_{k=3}^8 |U_{1k}|^2 = 0.65,$$

$$\begin{aligned} \psi_2^c = & 0.47 |5s_{1/2}(0,1)\rangle - 0.17 |5s_{1/2}(1,1)\rangle \\ & + \sum_{k=3}^8 U_{2k} |4d\epsilon l\rangle, \end{aligned}$$

where

$$\sum_{k=3}^8 |U_{2k}|^2 = 0.75,$$

$$\begin{aligned} \psi_3^c = & 0.55 |5s_{1/2}(0,1)\rangle + 0.03 |5s_{1/2}(1,1)\rangle \\ & + \sum_{k=3}^8 U_{3k} |4d\epsilon l\rangle, \end{aligned}$$

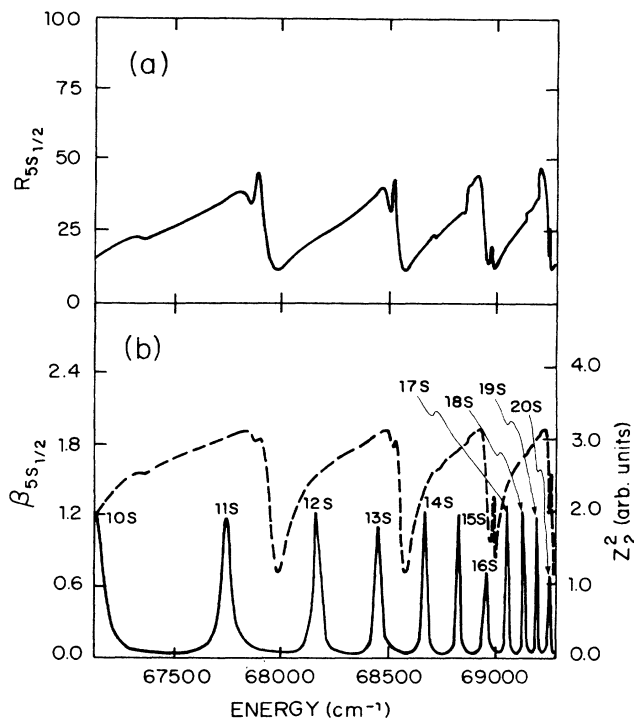


FIG. 11. (a) Calculations of  $R_{5s_{1/2}}$  for the  $5p_{1/2}ns_{1/2}$  series. Note the evident variations at the locations of the  $5p_{3/2}ns_{1/2}$  states. (b) The asymmetry parameter for the  $5p_{1/2}ns_{1/2}$  states,  $\beta_{5s_{1/2}}$  (---) and the spectral density, of  $\sum Z_{2\rho}^2$ , of the  $5p_{1/2}ns_{1/2}$  channel (—). The variations in  $\beta_{5s_{1/2}}$  and  $R_{5s_{1/2}}$  occur at the locations of the  $5p_{3/2}ns_{1/2}$  states.

where

$$\sum_{k=3}^8 |U_{3k}|^2 = 0.70.$$

As we have already mentioned, it is difficult to extract detailed information about the autoionization to the  $\text{Sr}^+ 4d_{3/2}$  and  $4d_{5/2}$  states from the angular distributions to the  $\text{Sr}^+ 4d_{3/2}$  and  $4d_{5/2}$  states because electrons corresponding to autoionization to both ion states are observed together. However, using the angular-momentum-transfer approach we can draw some qualitative conclusions from the observed angular distributions.

From Eq. (10) we can immediately determine the possible angular distributions for electrons ejected as pure  $p$  waves and as pure  $f$  waves, and these are given in Table VI. Since the observed asymmetry parameters  $\beta_{4d_j}$  are always greater than 0.2, which cannot occur with the ejection of only  $p$  electrons, a reasonable fraction of the autoionization results in ejected  $f$  electrons. In fact, the data are not inconsistent with the ejection of only  $f$  electrons. It is interesting to note that this octopole or exchange quadrupole process, in which three units of angular momenta are transferred to the ejected electron, is roughly as probable as the dipole process in which only one unit is transferred.

**E. Analysis of Sr  $5p_{3/2}ns_{1/2}$   $J=1$  autoionizing states lying above the Sr<sup>+</sup>  $5p_{1/2}$  limit**

The Sr  $5p_{3/2}ns_{1/2}$   $J=1$  autoionizing states for  $n > 15$  lie above the Sr<sup>+</sup>  $5p_{1/2}$  limit, and this opens two more decay channels,  $5p_{1/2}\epsilon s_{1/2}$  and  $5p_{1/2}\epsilon d_{3/2}$ , i.e., the ejection of  $s$  or  $d$  electrons in autoionization to the Sr<sup>+</sup>  $5p_{1/2}$  state. Since we have already included these interchannel couplings, there is in principal no new information in this energy range, but it does provide a valuable consistency check.

We begin with the results of the previous six-channel MQDT analysis.<sup>17</sup> The autoionization rate of state  $j$  to continuum  $i$  is proportional to  $R_{ji}^2$ . Thus a sensible first approximation to the branching ratio of the  $5p_{3/2}ns_{1/2}$  states to the  $5p_{1/2}$  state of Sr<sup>+</sup> is

$$R_{5p_{1/2}} \approx \frac{R_{12}^2 + R_{13}^2}{R_{12}^2 + R_{13}^2 + R_{14}^2}. \quad (27)$$

Using the previously determined values of  $R_{ij}$  Eq. (27) yields  $R_{5p_{1/2}} = 14.9\%$ . This value is in reasonable agreement with the value, 11.4%, calculated in a more exact fashion. The difference is due to the fact that the expression of Eq. (27) omits any interference effects between autoionization to the  $5p_{1/2}\epsilon s_{1/2}$  and  $5p_{1/2}\epsilon d_{3/2}$  channels. Not only does this interference affect the branching ratio, but also angular distributions, which are less amenable to meaningful qualitative estimates.

To analyze the  $5p_{3/2}ns_{1/2}$  states above the  $p_{1/2}$  limit we return to our six-channel MQDT model which now has only one closed and five open channels. Correspondingly there are also five eigenchannels, the phase shifts of which are obtained by solving the quintic equation resulting from Eq. (16). In addition, the  $U$  matrix relating the  $\psi_1^c$  and  $J_{cs}$  continua is now  $10 \times 10$  due to the addition of the  $5p_{1/2}\epsilon s_{1/2}$  and  $5p_{1/2}\epsilon d_{3/2}$  continua. Note, however, that these two channels which we labeled  $\psi_4^c$  and  $\psi_5^c$ , respectively, are the  $5p_{1/2}(1,0)$  and  $5p_{1/2}(1,2)$  channels, respectively, in the  $(J_{cs}, l)$  notation of Eq. (17).

If we construct an equation analogous to Eq. (17),

$$\begin{pmatrix} \psi_1^c \\ \psi_2^c \\ \psi_3^c \\ \psi_4^n \\ \psi_5^n \\ \psi_6^n \\ \psi_7^n \\ \psi_8^n \\ \psi_4^c \\ \psi_5^c \end{pmatrix} = U \begin{pmatrix} 5s_{1/2}(0,1) \\ 5s_{1/2}(1,1) \\ 4d_{3/2}(1,1) \\ 4d_{3/2}(2,1) \\ 4d_{3/2}(2,3) \\ 4d_{5/2}(2,1) \\ 4d_{5/2}(2,3) \\ 4d_{5/2}(3,3) \\ 5p_{1/2}(1,0) \\ 5p_{1/2}(1,2) \end{pmatrix}, \quad (28)$$

we have the same  $8 \times 8$  matrix as before with two added rows and columns, the only nonzero elements of which are  $U_{99} = U_{10,10} = 1$ . Since the  $U$  matrix elements of the original  $8 \times 8$  portion have been determined by analyzing the data from below the  $5p_{1/2}$  limit, and all the new ele-

TABLE VI. Allowed asymmetry parameters for autoionization to the  $4d_j$  cores with the ejection of only  $p$  and  $f$  electrons.

Ion core	$p$ electrons	$f$ electrons
$4d_{3/2}$	$-1.0 \leq \beta_{4d_{3/2}} \leq 0.2$	$\beta_{4d_{3/2}} = 0.8$
$4d_{5/2}$	$\beta_{4d_{5/2}} = 0.2$	$-1.0 \leq \beta_{4d_{5/2}} \leq 0.8$

ments are known, there is in principle nothing new in this energy range. However, it does provide a consistency check on the MQDT analysis of the interchannel interactions observed in the total photoexcitation spectra. With this in mind, let us focus on the new aspect of this region above the  $5p_{1/2}$  limit, autoionization to the  $5p_{1/2}$  state of Sr<sup>+</sup>. Using Eqs. (6) and (10) we can express the angular distribution for autoionization to the Sr<sup>+</sup>  $5p_{1/2}$  state as

$$\beta_{5p_{1/2}} = \frac{\{|S_2(J_t)|^2 - \sqrt{2}[S_2(J_t)S_0^\dagger(J_t) + S_2^\dagger(J_t)S_0(J_t)]\}}{[|S_2(J_t)|^2 + |S_0(J_t)|^2]}. \quad (29)$$

Note that  $J=1$ ; there is no parity-unfavored contribution. Similarly, using Eq. (7) we can express the cross section as

$$\sigma_{5p_{1/2}} = \frac{3\lambda^2}{4\pi} [ |S_2(J_t)|^2 + |S_0(J_t)|^2 ], \quad (30)$$

where the scattering matrix elements  $S_l(J_t)$  can be evaluated from Eqs. (14) and (17) as

$$S_2(1) = \left( \frac{4\pi\alpha\hbar\omega^3}{3^3c^2} \right)^{1/2} \langle \phi_1 \| D \| J_0 \rangle e^{i\sigma_{1/2,2}} \sum_p Z_{3p} Z_{1p} e^{i\tau_p}, \quad (31)$$

$$S_0(1) = \left( \frac{4\pi\alpha\hbar\omega^3}{3^3c^2} \right)^{1/2} \langle \phi_1 \| D \| J_0 \rangle e^{i\sigma_{1/2,0}} \sum_p Z_{2p} Z_{1p} e^{i\tau_p}. \quad (32)$$

In Eq. (29) the difference of the radial phase for the  $s$ - and  $d$ -wave electrons enters. Either from the properties of arguments of the  $\Gamma$  function<sup>25</sup> or the method used by Dill<sup>3</sup> it may be shown that

$$\cos(\sigma_{J_c, J_t+1} - \sigma_{J_c, J_t-1}) = \frac{\sqrt{[J_t(J_t+1) - (Z/W)^2]}}{\sqrt{\{[(J_t+1)^2 + (Z/W)^2][J_t^2 + (Z/W)^2]\}}}. \quad (33)$$

Here  $W$  is the kinetic energy of the escaping electron in a.u. and  $Z$  is the atomic number seen by the outer electron ( $Z=1$  in this case). For autoionization to the Sr<sup>+</sup>  $5p_{1/2}$  state  $J_c = \frac{1}{2}$ ,  $J_t = 1$ , and the electron kinetic energy is less than 60 meV, so  $W \ll 1$ , and  $\sigma_{1/2,2} - \sigma_{1/2,0} \approx \pi$ . From Eqs. (29) and (30),  $\beta_{5p_{1/2}}$  and  $R_{5p_{1/2}}$  can be obtained yielding values of

$$\beta_{5p_{1/2}} = 1.56 ,$$

$$R_{5p_{1/2}} = 11.4\% ,$$

in reasonable agreement with the experimental values of 1.4% and 8%. Thus the detailed angular-distribution measurements and the MQDT analysis of the interchannel interaction in the total photoexcitation spectra lead to the same conclusions. It is also interesting to note that  $\beta_{5p_{1/2}} > 1$  requires that  $s$  and  $d$  electrons be ejected, for only  $d$  electrons would lead to  $\beta_{5p_{1/2}} = 1$ ; only  $s$  electrons would lead to  $\beta_{5p_{1/2}} = 0$ . Thus the interference effects mentioned earlier are most pronounced in the angular distributions.

For the autoionization of the Sr  $5p_{3/2}ns_{1/2}$  states to the Sr<sup>+</sup>  $5s_{1/2}$  ion state, one obtains the same expressions as Eqs. (14) and (18), differing only in the fact that there are now five eigenchannels over which the  $\rho$  summation must be carried out. While there are five open collision channels, two of them are the  $5p_{1/2}\epsilon s_{1/2}$  and  $5p_{1/2}\epsilon d_{3/2}$  continua, so the summation over  $i$  is only over three channels.

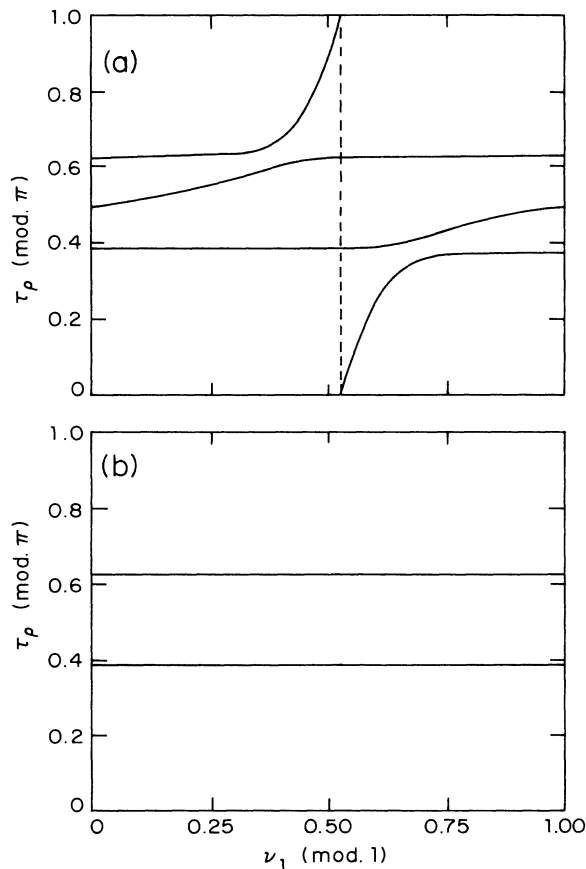


FIG. 12. (a) and (b) are the calculated eigenphase shifts  $\tau_p$  plotted as functions of  $\nu_1$  (modulo 1) by the six-channel MQDT model which can be transformed into an equivalent two-channel MQDT model due to the existence of only one bound channel.

A final interesting aspect of the region above the  $5p_{1/2}$  limit, where there is only one closed channel, is that the five interacting continua,  $\psi_i^c$  of our six-channel model, can be replaced by one interacting continuum. In this case we have only one  $i$  channel and one  $\rho$  channel, and the  $i$  and  $\rho$  sums of Eqs. (14) and (18) collapse to single terms, leaving only the energy-independent  $U$  matrix elements in the  $\beta_c$  and  $R_c$  expressions. Thus the  $\beta_c$  and  $R_c$  values must be energy independent. In fact this is true in our five continuum model as shown by Figs. 12 and 13. In Fig. 12 we show five eigenphases  $\tau_p$  plotted versus  $\nu_1$  (mod 1), the effective quantum number relative to the  $p_{3/2}$  limit. As expected all show a shift at  $\nu_1 = 0.55$ , the location of the  $5p_{3/2}ns_{1/2}$  states. This is reflected in the variation of the closed state density  $\Sigma |Z_{1\rho}|^2$  shown in Fig. 13(b). In Fig. 13(a) we show  $\beta_{5p_{1/2}}$  and  $\beta_{5s_{1/2}}$  which are constant. We recall that this result is valid for the case of one closed channel coupled to one interacting continuum. If there are two closed channels, which interact or may both be excited, there are necessarily two interacting continua,<sup>24,26</sup> and  $\beta_c$  and  $R_c$  are not energy independent. In fact these two apparently different cases are equivalent and are simply the differing parameters arising from a different choice of bases for the closed collision channels. In any event a variation in  $\beta_c$  and  $R_c$  periodic in the effective quantum number would be expected in this case.

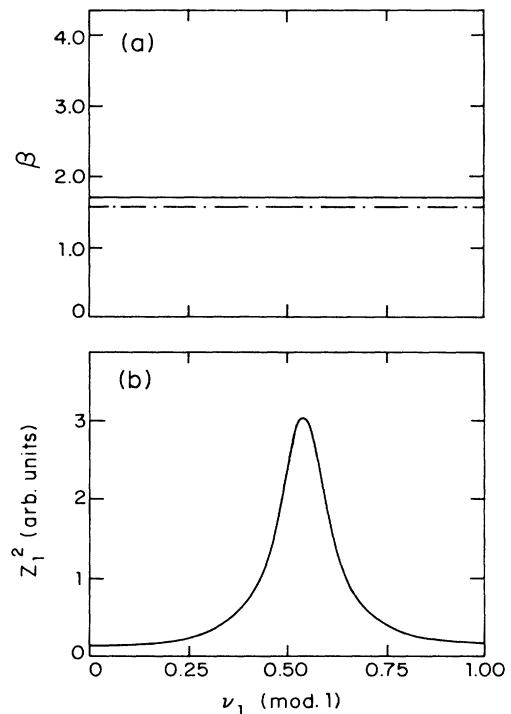


FIG. 13. (a) Asymmetry parameters  $\beta_{5s_{1/2}}$  and  $\beta_{5p_{1/2}}$  for the  $5p_{3/2}ns_{1/2}$   $J=1$  autoionizing states above the Sr<sup>+</sup>  $5p_{1/2}$  limit,  $\beta_{5s_{1/2}}$  (—) and  $\beta_{5p_{1/2}}$  (---). Note that both are energy independent. (b) The calculated density of the state  $Z_1^2$  for the bound  $5p_{3/2}ns_{1/2}$  channel.  $\nu_1$  is the effective quantum number plotted modulo 1.

## V. CONCLUSION

In this paper we have presented the results of measurements and analysis of the energy and angular distributions of the electrons ejected from the autoionization of Sr  $5p_{3/2}ns_{1/2}$  and  $5p_{1/2}ns_{1/2}$  odd-parity  $J=1$  doubly excited states.

The measurements themselves are similar to previous measurements made on Ba  $6pns$   $J=1$  autoionizing states,<sup>14-16</sup> so it is of interest to compare them. The most striking difference is in the branching ratio of states above the  $p_{1/2}$  states of the ion to the  $p_{1/2}$  ion core. For the Ba  $6p_{3/2}ns_{1/2}$  states  $R_{6p_{1/2}}$  is  $\sim 40-70\%$  while for the Sr  $5p_{3/2}ns_{1/2}$  states  $R_{5p_{1/2}} \sim 10\%$ . This is of course reflected in the different MQDT parameters for these two series. For Sr,  $R_{12}=0.16$ ,  $R_{13}=0.10$ , and  $R_{14}=0.45$  while for Ba,  $R_{12}=0.17$ ,  $R_{13}=0.42$ , and  $R_{14}=0.33$ . On the other hand, it is interesting to note that for both the Ba  $6p_{3/2}ns_{1/2}$  and Sr  $5p_{3/2}ns_{1/2}$  states the asymmetry parameter is approximately 1.5, indicating a similar fraction of  $s$  and  $d$  ejected electrons. The other difference between the Ba  $6pns$  and Sr  $5pns$  states is that the latter are more likely to autoionize to the Sr<sup>+</sup>  $4d_j$  cores,  $R_{4d_j} \sim 70\%$ , than the former are to autoionize to the Ba<sup>+</sup>  $5d_j$  cores,  $R_{5d_j} \sim 20\%$ . Yet it is still true that in both cases the asymmetry parameters for autoionization to these ion states is greater than 1, indicating a substantial fraction of ejected  $f$  electrons. Now that these extensive sets of measurements have been

made it would be of value to carry out *ab initio* calculations to see if the origin of the similarities and differences can be unearthed.

In addition, in this analysis, we have extended previous MQDT methods to allow the interpretation of these data in terms of elements of an energy-independent unitary transformation matrix  $U$  connecting different representations of the available continua. Using the approach it is straightforward to show that with our excitation method autoionizing states decaying into one continuum have asymmetry parameters and branching ratios which depend only on the  $U$  matrix elements and are thus constant across the autoionizing state. While this is rarely the case for excitation from the ground state it is true in the measurements reported here. On the other hand, the asymmetry parameters and branching ratios show clear variations in the regions where there is interaction between two series of autoionizing states and this in fact allows us to determine the signs of  $U$  matrix elements. In sum, this experimental and theoretical approach together comprise an excellent way to study autoionization.

## ACKNOWLEDGMENTS

It is a pleasure to acknowledge many useful discussions with O. C. Mullins, W. Sandner, R. R. Jones, and R. Kachru. This work was supported by the U.S. Department of Energy, Office of Basic Energy Sciences, Division of Chemical Sciences.

<sup>1</sup>U. Fano, Phys. Rev. **124**, 1866 (1961).

<sup>2</sup>J. A. R. Samson and J. L. Gardner, Phys. Rev. Lett. **31**, 1327 (1973).

<sup>3</sup>D. Dill, Phys. Rev. A **7**, 7 (1973).

<sup>4</sup>W. E. Cooke, T. F. Gallagher, S. A. Edelstein, and R. M. Hill, Phys. Rev. Lett. **40**, 178, (1978).

<sup>5</sup>M. J. Seaton, Rep. Prog. Phys. **46**, 167 (1983).

<sup>6</sup>U. Fano, Phys. Rev. A **2**, 353 (1970).

<sup>7</sup>K. T. Lu, Phys. Rev. A **4**, 579 (1971).

<sup>8</sup>W. E. Cooke and C. L. Cromer, Phys. Rev. A **32**, 2725 (1985).

<sup>9</sup>A. Giusti-Suzor and U. Fano, J. Phys. B **17**, 215 (1984).

<sup>10</sup>J. A. Armstrong, P. Esherick, and J. J. Wynne, Phys. Rev. A **15**, 180 (1977).

<sup>11</sup>M. Aymar and O. Robaux, J. Phys. B **12**, 531 (1979).

<sup>12</sup>W. E. Cooke and S. A. Bhatti, Phys. Rev. A **26**, 391 (1982).

<sup>13</sup>F. Gounand, T. F. Gallagher, W. Sandner, K. A. Safinya, and R. Kachru, Phys. Rev. A **27**, 1925 (1983).

<sup>14</sup>W. Sandner, R. Kachru, K. A. Safinya, F. Gounand, W. E. Cooke, and T. F. Gallagher, Phys. Rev. A **27**, 1717 (1983).

<sup>15</sup>R. Kachru, N. H. Tran, P. Pillet, and T. F. Gallagher, Phys.

Rev. A **29**, 2640 (1984).

<sup>16</sup>W. Sandner, U. Eichmann, V. Lange, and M. Volkel, J. Phys. B **19**, 51 (1986).

<sup>17</sup>E. Y. Xu, Y. Zhu, O. C. Mullins, and T. F. Gallagher, Phys. Rev. A **33**, 2401 (1986).

<sup>18</sup>C. N. Yang, Phys. Rev. **74**, 764 (1948).

<sup>19</sup>C. E. Moore, *Atomic Energy Levels*, Natl. Bur. Stand. (U.S.) Circ. No. 467 (U.S. GPO, Washington, D.C., 1947).

<sup>20</sup>U. Fano and D. Dill, Phys. Rev. A **6**, 185 (1972).

<sup>21</sup>D. Dill and U. Fano, Phys. Rev. Lett. **29**, 1203 (1972).

<sup>22</sup>C. M. Lee and K. T. Lu, Phys. Rev. A **8**, 241 (1973).

<sup>23</sup>O. C. Mullins, Y. Zhu, E. Y. Xu, and T. F. Gallagher, Phys. Rev. A **32**, 3234 (1985).

<sup>24</sup>L. Van Woerkom and W. E. Cooke, Phys. Rev. Lett. **57**, 1711 (1986).

<sup>25</sup>M. Abramowitz and I. A. Stegun, *Handbook of Mathematical Functions* (Dover, New York, 1972).

<sup>26</sup>R. Kachru, H. B. Van Linden van den Heuvell, and T. F. Gallagher, Phys. Rev. A **31**, 700 (1985).